Prepared for submission to JCAP

The Simons Observatory: Science Goals and Forecasts for the Enhanced Large Aperture Telescope

The Simons Observatory Collaboration

M. Abitbol,[1] **I. Abril-Cabezas,**[2,3] **S. Adachi,**[4,5,6] **P. Ade,**[7] **A. E. Adler,**[8,9] **P. Agrawal,**[10] **J. Aguirre,**[11] **Z. Ahmed,**[12,13] **S. Aiola,**[14] **T. Alford,**[15,16] **A. Ali,**[8] **D. Alonso,**[1] **M. A. Alvarez,**[9] **R. An,**[17] **K. Arnold,**[18,10] **P. Ashton,**[8,19,6] **Z. Atkins,**[20] **J. Austermann,**[21] **S. Azzoni,**[20,1] **C. Baccigalupi,**[22,23,24] **A. Baleato Lizancos,**[8,9] **D. Barron,**[25] **P. Barry,**[7] **J. Bartlett,**[26] **N. Battaglia,**[27] **R. Battye,**[28] **E. Baxter,**[29] **A. Bazarko,**[20] **J. A. Beall,**[21] **R. Bean,**[27] **D. Beck,**[30] **S. Beckman,**[8] **J. Begin,**[20] **A. Beheshti,**[31] **B. Beringue,**[26] **T. Bhandarkar,**[11] **S. Bhimani,**[15] **F. Bianchini,**[32] **E. Biermann,**[31] **S. Biquard,**[26] **B. Bixler,**[10] **S. Boada,**[33] **D. Boettger,**[10] **B. Bolliet,**[34,3] **J. R. Bond,**[35] **J. Borrill,**[19,36,8] **J. Borrow,**[11] **C. Braithwaite,**[7] **T. L. R. Brien,**[7] **M. L. Brown,**[28] **S. M. Bruno,**[20] **S. Bryan,**[37] **R. Bustos,**[38] **H. Cai,**[31] **E. Calabrese,**[7] **V. Calafut,**[27] **F. M. Carl,**[20] **A. Carones,**[22] **J. Carron,**[39] **A. Challinor,**[40,2,3] **P. Chanial,**[26] **N. Chen,**[41] **K. Cheung,**[28] **B. Chiang,**[42] **Y. Chinone,**[43,6] **J. Chluba,**[28] **H. S. Cho,**[12,13] **S. K. Choi,**[44] **M. Chu,**[10] **J. Clancy,**[32] **S. E. Clark,**[30,12] **P. Clarke,**[2,3] **J. Cleary,**[15] **D. L. Clements,**[45] **J. Connors,**[21] **C. Contaldi,**[45] **G. Coppi,**[46] **L. Corbett,**[8] **N. F. Cothard,**[47] **W. Coulton,**[3,2] **K. D. Crowley,**[20] **K. T. Crowley,**[10,8] **A. Cukierman,**[12,30,8] **J. M. D'Ewart,**[13] **K. Dachlythra,**[46] **R. Datta,**[15] **S. Day-Weiss,**[20] **T. de Haan,**[48] **M. Devlin,**[11] **L. Di Mascolo,**[49] **S. Dicker,**[11] **B. Dober,**[21] **C. Doux,**[11] **P. Dow,**[50] **S. Doyle,**[7] **C. J. Duell,**[51] **S. M. Duff,**[21] **A. J. Duivenvoorden,**[52,14,20] **J. Dunkley,**[20,53] **D. Dutcher,**[20] **R. Dünner,**[54] **M. Edenton,**[50] **H. El Bouhargani,**[20,19] **J. Errard,**[26] **G. Fabbian,**[7] **V. Fanfani,**[46] **G. S. Farren,**[19] **J. Fergusson,**[2,3] **S. Ferraro,**[19,8] **R. Flauger,**[10]

[1]Author contributions to this paper can be found at https://simonsobservatory.org/wp-content/uploads/2025/03/Author-contribution-statement-20250228.pdf.

A. Foster,[20] **K. Freese,**[55,56,57] **J. C. Frisch,**[12] **A. Frolov,**[58] **G. Fuller,**[10]
N. Galitzki,[56,57] **P. A. Gallardo,**[11,59] **J. T. Galvez Ghersi,**[58]
K. Ganga,[26] **J. Gao,**[21] **X. Garrido,**[60] **E. Gawiser,**[33] **M. Gerbino,**[61,62]
R. Gerras,[17] **S. Giardiello,**[7] **A. Gill,**[63] **V. Gilles,**[28] **U. Giri,**[64]
E. Gleave,[45] **V. Gluscevic,**[17] **N. Goeckner-Wald,**[8] **J. E. Golec,**[16,59]
S. Gordon,[37] **M. Gralla,**[65] **S. Gratton,**[40] **D. Green,**[10] **J. C. Groh,**[9]
C. Groppi,[37] **Y. Guan,**[66,67] **N. Gupta,**[32] **J. E. Gudmundsson,**[68,55]
S. Hagstotz,[55] **P. Hargrave,**[7] **S. Haridas,**[11] **K. Harrington,**[69,15]
I. Harrison,[7,28] **M. Hasegawa,**[48] **M. Hasselfield,**[14] **V. Haynes,**[28]
M. Hazumi,[48,6] **A. He,**[17] **E. Healy,**[59] **S. W. Henderson,**[12,13]
B. S. Hensley,[70] **E. Hertig,**[40,3] **C. Hervías-Caimapo,**[54] **M. Higuchi,**[71]
C. A. Hill,[8,19] **J. C. Hill,**[72,14] **G. Hilton,**[21] **M. Hilton,**[73,74]
A. D. Hincks,[67,75] **G. Hinshaw,**[76] **R. Hložek,**[67,66] **A. Y. Q. Ho,**[51]
S. Ho,[14] **S. P. Ho,**[30] **T. D. Hoang,**[77] **J. Hoh,**[37] **E. Hornecker,**[67]
A. L. Hornsby,[28] **S. C. Hotinli,**[64] **Z. Huang,**[78] **Z. B. Huber,**[51]
J. Hubmayr,[21] **K. Huffenberger,**[79,80,42] **J. P. Hughes,**[33]
A. Idicherian Lonappan,[10] **M. Ikape,**[67,66] **K. Irwin,**[12,30,13] **J. Iuliano,**[11]
A. H. Jaffe,[45] **B. Jain,**[11] **H. T. Jense,**[7] **O. Jeong,**[8] **A. Johnson,**[10]
B. R. Johnson,[50] **M. Johnson,**[64] **M. Jones,**[1] **B. Jost,**[6,81]
D. Kaneko,[48] **E. D. Karpel,**[30] **Y. Kasai,**[5] **N. Katayama,**[6]
B. Keating,[10] **B. Keller,**[51] **R. Keskitalo,**[36,82,10] **J. Kim,**[11]
T. Kisner,[36,82] **K. Kiuchi,**[71] **J. Klein,**[11] **K. Knowles,**[74]
A. M. Kofman,[11,15,59] **B. J. Koopman,**[83] **A. Kosowsky,**[31] **R. Kou,**[84]
N. Krachmalnicoff,[22] **D. Kramer,**[65] **A. Krishak,**[17] **A. Krolewski,**[8]
A. Kusaka,[71,19,6] **A. Kusiak,**[40,3] **P. La Plante,**[85] **A. La Posta,**[1]
A. Laguë,[11] **J. Lashner,**[83,17] **M. Lattanzi,**[61,62] **A. Lee,**[8,19] **E. Lee,**[11,28]
J. Leech,[1] **C. Lessler,**[16,59] **J. S. Leung,**[45] **A. Lewis,**[84] **Y. Li,**[51]
Z. Li,[86,9,35] **M. Limon,**[11] **L. Lin,**[51] **M. Link,**[21] **J. Liu,**[6,81] **Y. Liu,**[20]
J. Lonergan,[17] **T. Louis,**[60] **T. Lucas,**[21] **M. Ludlam,**[82] **M. Lungu,**[87]
M. Lyons,[7] **N. MacCrann,**[40] **A. MacInnis,**[88] **M. Madhavacheril,**[11]
D. Mak,[45] **F. Maldonado,**[42] **M. Mallaby-Kay,**[15] **A. Manduca,**[11]
A. Mangu,[16] **H. Mani,**[37] **A. S. Maniyar,**[12,13] **G. A. Marques,**[89]
J. Mates,[21] **T. Matsumura,**[6,81,71] **P. Mauskopf,**[37] **A. May,**[28]
N. McCallum,[28] **H. McCarrick,**[20] **F. McCarthy,**[2,3,14]
M. McCulloch,[28] **J. McMahon,**[15,59,16,90,89] **P. D. Meerburg,**[91]
Y. Mehta,[37] **J. Melin,**[26,92] **J. Meyers,**[93] **A. Middleton,**[51] **A. Miller,**[17]
M. Mirmelstein,[84] **K. Moodley,**[74] **J. Moore,**[94] **M. Morshed,**[62]
T. Morton,[17] **E. Moser,**[51] **T. Mroczkowski,**[95] **M. Murata,**[71]
M. Münchmeyer,[96] **S. Naess,**[97] **H. Nakata,**[5] **T. Namikawa,**[2,6,81,3]

M. Nashimoto,[71] **F. Nati,**[46] **P. Natoli,**[62,61] **M. Negrello,**[7]
S. K. Nerval,[67,66] **L. Newburgh,**[83] **D. V. Nguyen,**[83] **A. Nicola,**[98,53]
M. D. Niemack,[51,27] **H. Nishino,**[71] **Y. Nishinomiya,**[71] **A. Orlando,**[28]
J. Orlowski-Scherer,[11] **L. Pagano,**[62,61,99] **L. A. Page,**[20] **S. Pandey,**[72,11]
A. Papageorgiou,[7] **I. Paraskevakos,**[20] **B. Partridge,**[100] **R. Patki,**[27]
M. Peel,[45] **K. Perez Sarmiento,**[11] **F. Perrotta,**[22] **P. Phakathi,**[74]
L. Piccirillo,[28] **E. Pierpaoli,**[17] **T. Pinsonneault-Marotte,**[12,13]
G. Pisano,[101] **D. Poletti,**[22] **R. Puddu,**[54] **G. Puglisi,**[102,103,104]
F. J. Qu,[12,13] **M. J. Randall,**[10] **C. Ranucci,**[22] **C. Raum,**[8]
R. Reeves,[105] **C. L. Reichardt,**[32] **M. Remazeilles,**[106] **Y. Rephaeli,**[107]
D. Riechers,[27] **J. Robe,**[11] **M. F. Robertson,**[84] **N. Robertson,**[40]
K. Rogers,[67] **F. Rojas,**[54] **A. Romero,**[13] **E. Rosenberg,**[28] **A. Rotti,**[28]
S. Rowe,[7] **A. Roy,**[22] **S. Sadeh,**[107] **N. Sailer,**[8] **K. Sakaguri,**[71]
T. Sakuma,[20] **Y. Sakurai,**[108,6] **M. Salatino,**[30] **G. H. Sanders,**[87,109]
D. Sasaki,[71] **M. Sathyanarayana Rao,**[110] **T. P. Satterthwaite,**[30,12]
L. Saunders,[15,89] **L. Scalcinati,**[46] **E. Schaan,**[13,12] **B. Schmitt,**[11]
M. Schmittfull,[111] **N. Sehgal,**[88] **J. Seibert,**[10] **Y. Seino,**[20,5]
U. Seljak,[8,19] **S. Shaikh,**[37] **E. Shaw,**[56,57] **P. Shellard,**[2,3] **B. Sherwin,**[2,3]
M. Shimon,[107] **J. E. Shroyer,**[50,112] **C. Sierra,**[12,13] **J. Sievers,**[74]
C. Sifón,[113] **P. Sikhosana,**[74] **M. Silva-Feaver,**[83] **S. M. Simon,**[89]
A. Sinclair,[37] **K. Smith,**[64] **W. Sohn,**[26] **X. Song,**[8] **R. F. Sonka,**[20]
D. Spergel,[14,53] **J. Spisak,**[10] **S. T. Staggs,**[20] **G. Stein,**[8,19]
J. R. Stevens,[51] **R. Stompor,**[26] **E. Storer,**[20] **R. Sudiwala,**[7]
J. Sugiyama,[71] **K. M. Surrao,**[72] **S. Sutariya,**[16] **A. Suzuki,**[19]
J. Suzuki,[5] **O. Tajima,**[5] **S. Takakura,**[5,6] **A. Takeuchi,**[71] **I. Tansieri,**[55]
A. C. Taylor,[1] **G. Teply,**[10] **T. Terasaki,**[71] **A. Thomas,**[15]
D. B. Thomas,[28] **R. Thornton,**[11] **H. Trac,**[41] **T. Tsan,**[19]
E. Tsang King Sang,[26] **C. Tucker,**[7] **J. Ullom,**[21] **L. Vacher,**[22]
L. Vale,[21] **A. van Engelen,**[37] **J. Van Lanen,**[21] **J. van Marrewijk,**[95,114]
D. D. Van Winkle,[13] **C. Vargas,**[79,80,54] **E. M. Vavagiakis,**[94,51]
I. Veenendaal,[7] **C. Vergès,**[26] **M. Vissers,**[21] **M. Viña,**[7]
K. Wagoner,[115,20] **S. Walker,**[21] **L. Walters,**[50] **Y. Wang,**[51,20]
B. Westbrook,[8] **J. Williams,**[28] **P. Williams,**[19] **H. Winch,**[67]
E. J. Wollack,[116] **K. Wolz,**[1] **J. Wong,**[28] **Z. Xu,**[117] **K. Yamada,**[20,71]
E. Young,[12,30] **B. Yu,**[8] **C. Yu,**[12,30] **M. Zannoni,**[46] **K. Zheng,**[20]
N. Zhu,[11] **A. Zonca,**[118] **and I. Zubeldia**[40,28]

[1]Department of Physics, University of Oxford, Denys Wilkinson Building, Keble Road, Oxford OX1 3RH, United Kingdom

[2]DAMTP, Centre for Mathematical Sciences, University of Cambridge, Wilberforce Road, Cambridge CB3 OWA, UK

[3]Kavli Institute for Cosmology Cambridge, Madingley Road, Cambridge CB3 0HA, UK
[4]Hakubi Center for Advanced Research, Kyoto University, Kyoto 606-8501, Japan
[5]Department of Physics, Faculty of Science, Kyoto University, Kyoto 606-8502, Japan
[6]Kavli IPMU (WPI), UTIAS, The University of Tokyo, Kashiwa, Chiba 277-8583, Japan
[7]School of Physics and Astronomy, Cardiff University, UK
[8]Department of Physics, University of California Berkeley, Berkeley, CA, USA
[9]Lawrence Berkeley National Laboratory, Berkeley, CA, USA
[10]Department of Physics, University of California San Diego, San Diego, CA, USA
[11]Department of Physics and Astronomy, University of Pennsylvania, Philadelphia, PA 19104 USA
[12]Kavli Institute for Particle Astrophysics & Cosmology, 452 Lomita Mall, Stanford, CA 94305, USA
[13]SLAC National Accelerator Laboratory, 2575 Sand Hill Road, Menlo Park, California 94025, USA
[14]Center for Computational Astrophysics, Flatiron Institute, USA
[15]University of Chicago, Department of Astronomy and Astrophysics, 5720 S Ellis Ave, Chicago, IL, 60637, USA
[16]University of Chicago, Department of Physics, 5720 S Ellis Ave, Chicago, IL, 60637, USA
[17]Department of Physics and Astronomy, University of Southern California, Los Angeles, CA 90089-1483 USA
[18]Department of Astronomy & Astrophysics, University of California San Diego, San Diego, CA, USA
[19]Physics Division, Lawrence Berkeley National Laboratory, Berkeley, CA, USA
[20]Department of Physics, Princeton University, Jadwin Hall, Princeton, NJ 08544, USA
[21]Quantum Sensors Division, National Institute of Standards and Technology, 325 Broadway, Boulder, CO 80305
[22]The International School for Advanced Studies (SISSA), via Bonomea 265, I-34136 Trieste, Italy
[23]The National Institute for Nuclear Physics (INFN), via Valerio 2, I-34127, Trieste, Italy
[24]Institute for Fundamental Physics of the Universe (IFPU), Via Beirut 2, 34151, Trieste, Italy
[25]Department of Physics and Astronomy, University of New Mexico, USA
[26]Université Paris Cité, CNRS, Astroparticule et Cosmologie, F-75013 Paris, France
[27]Department of Astronomy, Cornell University, Ithaca, NY 14853, USA
[28]Jodrell Bank Centre for Astrophysics, Department of Physics and Astronomy, University of Mancheseter, Manchester M13 9PL, UK
[29]Institute for Astronomy, University of Hawai'i, 2680 Woodlawn Drive, Honolulu, HI 96822, USA
[30]Department of Physics, Stanford University, USA
[31]Department of Physics and Astronomy, University of Pittsburgh
[32]School of Physics, The University of Melbourne, Parkville VIC 3010, Australia
[33]Department of Physics and Astronomy, Rutgers, the State University of New Jersey, Piscataway, NJ, USA

[34]Astrophysics Group, Cavendish Laboratory, J. J. Thomson Avenue, Cambridge CB3 0HE, United Kingdom
[35]Canadian Institute for Theoretical Astrophysics, University of Toronto, 60 St. George St., Toronto, ON M5S 3H4, Canada
[36]Computational Cosmology Center, Lawrence Berkeley National Laboratory, Berkeley, CA, USA
[37]School of Earth and Space Exploration, Arizona State University, Tempe, AZ, 85287
[38]Departamento de Ingeniería Eléctrica, Universidad Católica de la Santísima Concepción, Alonso de Ribera 2850, Concepción, Chile
[39]Université de Genève, Département de Physique Théorique et CAP, 24 Quai Ansermet, CH-1211 Genève 4, Switzerland
[40]Institute of Astronomy, University of Cambridge, Madingley Road, Cambridge CB3 0HA, UK
[41]McWilliams Center for Cosmology and Astrophysics, Department of Physics, Carnegie Mellon University, USA
[42]Department of Physics, Florida State University, Tallahassee, FL 32306 USA
[43]QUP (WPI), KEK, Tsukuba, Ibaraki 305-0801, Japan
[44]Department of Physics and Astronomy, University of California, Riverside, CA 92521, USA
[45]Imperial College London, Blackett Lab, Prince Consort Road, London SW7 2AZ, UK
[46]Department of Physics, University of Milano-Bicocca, Piazza della Scienza 3, 20126 Milano (MI), Italy
[47]Department of Applied and Engineering Physics, Cornell University, Ithaca, NY 14853, USA
[48]High Energy Accelerator Research Organization (KEK), Tsukuba, 305-0801, Japan
[49]Kapteyn Astronomical Institute, University of Groningen, Landleven 12, 9747 AD, Groningen, The Netherlands
[50]Department of Astronomy, University of Virginia, Charlottesville, VA 22904, USA
[51]Department of Physics, Cornell University, Ithaca, NY 14853, USA
[52]Max-Planck-Institut für Astrophysik, Karl-Schwarzschild Str. 1, 85741 Garching, Germany
[53]Department of Astrophysical Sciences, Payton Hall, Princeton University, Princeton, NJ 08544, USA
[54]Instituto de Astrofísica and Centro de Astro-Ingeniería, Facultad de Física, Pontificia Universidad Católica de Chile, Chile
[55]The Oskar Klein Centre for Cosmoparticle Physics, Department of Physics, Stockholm University, AlbaNova, SE-106 91 Stockholm, Sweden
[56]Department of Physics, University of Texas at Austin, Austin, TX, 78712, USA
[57]Weinberg Institute for Theoretical Physics, Texas Center for Cosmology and Astroparticle Physics, Austin, TX 78712, USA
[58]Physics Department, Simon Fraser University
[59]Kavli Institute for Cosmological Physics, University of Chicago, 5640 S Ellis Ave, Chicago, IL, 60637, USA
[60]Université Paris-Saclay, CNRS/IN2P3, IJCLab, 91405 Orsay, France
[61]Istituto Nazionale di Fisica Nucleare, Sezione di Ferrara, via Saragat 1, I-44122 Ferrara, Italy

[62]Dipartimento di Fisica e Scienze della Terra, Università degli Studi di Ferrara, via Saragat 1, I-44122 Ferrara, Italy
[63]Department of Aeronautics and Astronautics, Massachusetts Institute of Technology, 77 Massachusetts Avenue, Cambridge, MA 02139, USA
[64]Perimeter Institute for Theoretical Physics, 31 Caroline Street N, Waterloo ON N2L 2Y5, Canada
[65]Department of Astronomy/Steward Observatory, University of Arizona, 933 N. Cherry Ave., Tucson, AZ 85721, USA
[66]Dunlap Institute for Astronomy & Astrophysics, University of Toronto, 50 St. George St., Toronto ON M5S 3H4, Canada
[67]David A. Dunlap Department of Astronomy and Astrophysics, University of Toronto, 50 St. George St., Toronto ON M5S 3H4, Canada
[68]Science Institute, University of Iceland, 107 Reykjavik, Iceland
[69]Argonne National Laboratory, High Energy Physics Division. 9700 S Cass Ave, Lemont, IL, 60439, USA
[70]Jet Propulsion Laboratory, California Institute of Technology, 4800 Oak Grove Drive, Pasadena, CA 91109, USA
[71]Department of Physics, The University of Tokyo, Tokyo 113-0033, Japan
[72]Department of Physics, Columbia University, New York, NY 10027, USA
[73]Wits Centre for Astrophysics, School of Physics, University of the Witwatersrand, Private Bag 3, 2050, Johannesburg, South Africa
[74]Astrophysics Research Centre, School of Mathematics, Statistics, and Computer Science, University of KwaZulu-Natal, Westville Campus, Durban 4041, South Africa
[75]Specola Vaticana (Vatican Observatory), V-00120 Vatican City State
[76]Department of Physics and Astronomy, University of British Columbia, Vancouver, BC, Canada
[77]School of Physics and Astronomy, University of Minnesota, Minneapolis, MN 55455, USA
[78]School of Physics and Astronomy, Sun Yat-sen University, 2 Daxue Road, Zhuhai, 519082, China
[79]Department of Physics & Astronomy, Texas A&M University, College Station, TX 77843, USA
[80]Mitchell Institute for Fundamental Physics & Astronomy, Texas A&M University, College Station, TX 77843, USA
[81]Center for Data-Driven Discovery, Kavli IPMU (WPI), UTIAS, The University of Tokyo, Kashiwa, Chiba 277-8583, Japan
[82]Space Sciences Laboratory, University of California Berkeley, Berkeley, CA, USA
[83]Wright Laboratory, Department of Physics, Yale University, New Haven, Connecticut 06511, USA
[84]Department of Physics & Astronomy, University of Sussex, Brighton BN1 9QH, UK
[85]Nevada Center for Astrophysics, University of Nevada Las Vegas, Las Vegas, NV 89154, USA
[86]Berkeley Center for Cosmological Physics, University of California, Berkeley, CA 94720, USA
[87]Simons Observatory

[88]Physics and Astronomy Department, Stony Brook University, Stony Brook, NY 11794, USA
[89]Fermi National Accelerator Laboratory, Batavia, IL 60510, USA
[90]University of Chicago, Enrico Fermi Institute, 5640 S Ellis Ave, Chicago, IL, 60637, USA
[91]Van Swinderen Institute for particle physics and gravity, Nijenborgh 3, 9747 AG Groningen, The Netherlands
[92]Université Paris-Saclay, CEA, Département de Physique des Particules, 91191, Gif-sur-Yvette, France
[93]Department of Physics, Southern Methodist University, USA
[94]Department of Physics, Duke University, Durham, NC 27710, USA
[95]European Southern Observatory (ESO), Karl-Schwarzschild-Strasse 2, Garching 85748, Germany
[96]Department of Physics, University of Wisconsin-Madison, Madison, WI 53706, USA
[97]Institute for theoretical astrophysics, University of Oslo, Norway
[98]Argelander-Institut für Astronomie, Universität Bonn, Auf dem Hügel 71, 53121 Bonn, Germany
[99]Institut d'Astrophysique Spatiale, CNRS, Univ. Paris-Sud, Université Paris-Saclay, Bât. 121, 91405 Orsay cedex, France
[100]Department of Physics and Astronomy, Haverford College, 370 Lancaster Ave, Haverford, PA 19041, USA
[101]Department of Physics, Sapienza University of Rome
[102]Dipartimento di Fisica e Astronomia, Università degli Studi di Catania, via S. Sofia, 64, 95123, Catania, Italy
[103]The National Institute for Nuclear Physics INFN - Via S. Sofia 64, 95123 Catania, Italy
[104]INAF - Osservatorio Astrofisico di Catania, via S. Sofia 78, 95123 Catania, Italy
[105]Departamento de Astronomía, Universidad de Concepción, Victor Lamas 1290, Concepción, Chile
[106]Instituto de Fisica de Cantabria (CSIC-UC), Avenida de los Castros s/n, 39005 Santander, Spain
[107]School of Physics and Astronomy, Tel Aviv University, Tel Aviv, 69978, Israel
[108]Faculty of Engineering, Department of Mechanical and Electrical Engineering, 5000-1, Toyohira, Chino-shi, Nagano, 391-0292, Japan
[109]Project Science LLC, 572 Alta Vista Way, Laguna Beach, CA 92651 USA
[110]Raman Research Institute, Bengaluru, India
[111]PDT Partners, 60 Columbus Circle, New York, NY 10023, USA
[112]National Radio Astronomy Observatory, 520 Edgemont Road, Charlottesville, VA 22903, USA
[113]Instituto de Física, Pontificia Universidad Católica de Valparaíso, Casilla 4059, Valparaíso, Chile
[114]Leiden Observatory, Leiden University, P.O. Box 9513, 2300 RA Leiden, The Netherlands
[115]Department of Physics, North Carolina State University
[116]NASA / Goddard Space Flight Center, Greenbelt, MD 20771, USA
[117]MIT Kavli Institute, Massachusetts Institute of Technology, 77 Massachusetts Avenue, Cambridge, MA 02139, USA

[118]San Diego Supercomputer Center, University of California San Diego, La Jolla, CA, USA

E-mail: so_publications@simonsobservatory.org

Abstract. We describe updated scientific goals for the wide-field, millimeter-wave survey that will be produced by the Simons Observatory (SO). Significant upgrades to the 6–meter SO Large Aperture Telescope (LAT) are expected to be complete by 2028, and will include a doubled mapping speed with 30,000 new detectors and an automated data reduction pipeline. In addition, a new photovoltaic array will supply most of the observatory's power. The LAT survey will cover about 60% of the sky at a regular observing cadence, with five times the angular resolution and ten times the map depth of the *Planck* satellite. The science goals are to: (1) determine the physical conditions in the early universe and constrain the existence of new light particles; (2) measure the integrated distribution of mass, electron pressure, and electron momentum in the late-time universe, and, in combination with optical surveys, determine the neutrino mass and the effects of dark energy via tomographic measurements of the growth of structure at redshifts $z \lesssim 3$; (3) measure the distribution of electron density and pressure around galaxy groups and clusters, and calibrate the effects of energy input from galaxy formation on the surrounding environment; (4) produce a sample of more than 30,000 galaxy clusters, and more than 100,000 extragalactic millimeter sources, including regularly sampled AGN light-curves, to study these sources and their emission physics; (5) measure the polarized emission from magnetically aligned dust grains in our Galaxy, to study the properties of dust and the role of magnetic fields in star formation; (6) constrain asteroid regoliths, search for Trans-Neptunian Objects, and either detect or eliminate large portions of the phase space in the search for Planet 9; and (7) provide a powerful new window into the transient universe on time scales of minutes to years, concurrent with observations from the Vera C. Rubin Observatory of overlapping sky.

Contents

1 Introduction and overall goals

The millimeter-wave sky encodes information about the origins of the universe, the nature of gravity and other fundamental fields, the evolution of galaxies, the extent of our Solar System, and more. Unlocking this wealth of information requires large, well-characterized, multi-frequency maps with a large spatial dynamic range, high signal-to-noise, and good temporal coverage. The Simons Observatory (SO) is designed to make two surveys of the millimeter sky (Ade et al. 2019). A deep, lower-resolution survey will search for primordial gravitational waves (HEPAP Subcommittee Collaboration 2014, 2023), either detecting them or producing an unprecedented limit on a measure of their amplitude, the tensor-to-scalar ratio. A wide, higher-resolution survey of 25,000 deg^2 reaching a co-added noise level[1] of 2.6 μK $\cdot$ arcmin will have ten times the co-added map depth of the *Planck* satellite data with five times higher angular resolution (Planck Collaboration et al. 2020a), and will cover roughly sixteen times the area observed by the South Pole Telescope (SPT) 3G deep survey (Benson et al. 2014; Prabhu et al. 2024). Maps from the wide survey, made public on a regular schedule, can be used to address a broad set of questions in astronomy highlighted in the Decadal Survey on Astronomy and Astrophysics "Astro2020" White Papers, including the evolution of galaxies (Battaglia et al. 2019; De Zotti et al. 2019a), the role of magnetic fields in star formation in our Galaxy (Clark et al. 2019; Fissel et al. 2019), the properties of neutrinos and other light, relativistic particles (Alvarez et al. 2019; Green et al. 2019; Grin et al. 2019; Grohs et al. 2019), the characterization of primordial density perturbations (Gluscevic et al. 2019; Meerburg et al. 2019; Slosar et al. 2019b), and beyond (De Zotti et al. 2019b; Hensley et al. 2019; Holder et al. 2019; Slosar et al. 2019a).

The SO program is being enhanced in a number of ways beyond the capabilities described in Ade et al. (2019). This paper focuses on the 6-meter Large Aperture Telescope (LAT) and the science enabled via its wide-area, high-resolution survey. The improved capabilities include doubling the number of detectors in the focal plane of the SO LAT receiver, developing a robust data pipeline that enables rapid mapmaking and transient alerts delivered to the community, and installing a photovoltaic array at the site on Cerro Toco, in the Atacama Desert of Chile, to provide power to the observatory. This expansion, and an extended duration of the SO survey through 2034, will significantly enhance the experimental capabilities and scientific return of the SO LAT. Other planned additions to the SO program, which target primordial gravitational-wave science with Small Aperture Telescopes (SATs, Galitzki et al. 2024), will be described elsewhere.

The remainder of this paper is organized as follows. In Sec. 2, we briefly describe the expanded capabilities of the wide-field LAT survey. In Sec. 3, we forecast the primary scientific analyses that will be enabled by this program. Much of the forecasting methodology used here is similar or identical to that employed in the SO science goals and forecasts paper (Ade et al. 2019) or the complementary SO Galactic science goals and forecasts paper (Hensley et al. 2022), and we direct the interested reader to those papers for further details. In Sec. 4, we conclude and discuss the outlook for SO operations and science.

2 Expanded capabilities

The mapping speed for the wide survey with the SO LAT (Gudmundsson et al. 2021; Parshley et al. 2018) will be almost doubled by fully populating the LAT receiver (LATR; Zhu et al.

[1]Throughout this work, K denotes CMB thermodynamic temperature units.

Table 1. SO Large Aperture Telescope Survey Specifications

Frequency [GHz]	FWHM [arcmin]	Baseline Depth [$\mu K \cdot arcmin$]	Goal Depth [$\mu K \cdot arcmin$]	Frequency Bands	Detector Count	Optics Tubes
27 (22 – 30)	7.4	61	44	LF	354	1
39 (30 – 47)	5.1	30	23		354	
93 (77 – 104)	2.2	5.3	3.8	MF	20,640	8
145 (128 – 169)	1.4	6.6	4.1		20,640	
225 (198 – 256)	1.0	15	10	UHF	10,320	4
280 (256 – 313)	0.9	35	25		10,320	

Expected instrumental and map-depth properties for the fully completed, nine-year SO LAT survey (2025-2034). Two sensitivity targets are presented (baseline and goal), as in Ade et al. (2019). The values in parentheses in the first column represent the approximate passband width of each frequency channel.

2021) with six additional optics tubes (OTs), thus adding roughly 30,000 detectors.[2] The six new OTs will comprise four mid-frequency (MF) OTs containing dichroic detectors with bands centered at 93 and 145 GHz (Sierra et al. 2025), and two ultra-high-frequency (UHF) OTs containing dichroic detectors with bands centered at 225 and 280 GHz. After installation of these new detectors, the receiver will contain eight MF, four UHF, and one low-frequency (LF) OTs, containing a total of roughly 60,000 detectors and fully populating the receiver's available focal plane. The anticipated sensitivities of these detectors, including effects due to atmospheric noise, are described in Ade et al. (2019). The angular resolution of the LAT at these frequencies (e.g., FWHM $\approx$ 1.4 arcmin at 145 GHz) is also described there. Table 1 summarizes the frequency channels, resolution, sensitivity, and detector counts for the fully populated LATR. We note that these values reflect current best estimates derived from ongoing technical development of the SO LAT hardware, as well as the currently planned sky coverage of the SO LAT survey, which is wider than that assumed in Ade et al. (2019). Estimates of the bandwidth of each frequency channel are also provided, with each edge determined by the point at which the response drops to 50% of the peak. These are computed from the simulated optical coupling and on-chip filters. Further discussion of the sensitivities can be found in Appendix A, including the per-OT noise-equivalent temperatures (NETs).

The lack of reliable power at the 5,200-meter site on Cerro Toco in Chile has been a risk to the performance of all projects operating there over the past few decades. The expanded SO program includes the installation of a photovoltaic array at the site, which will reduce the reliance on diesel-generated power by 70% and provide a more stable power system. This will translate into improved sensitivity by increasing on-sky observation time (we estimate a 5–10% increase in uptime), while also decreasing our environmental impact.

The enhancement in hardware will be accompanied by substantial upgrades in the data processing pipeline to analyze and publicly deliver the data (see Guan et al. 2024, for recent work toward these goals). An open-source data pipeline will convert raw time-ordered data to maps of the sky and light curves of millimeter sources, to be released to the community.

These new components are planned to be complete by 2028 (see timeline in Fig. 1), while the initial SO survey is ongoing using the half-populated LATR (Haridas et al. 2024).

[2]The initial seven OTs in the LATR comprise one low-frequency, four mid-frequency, and two ultra-high-frequency OTs (Ade et al. 2019).

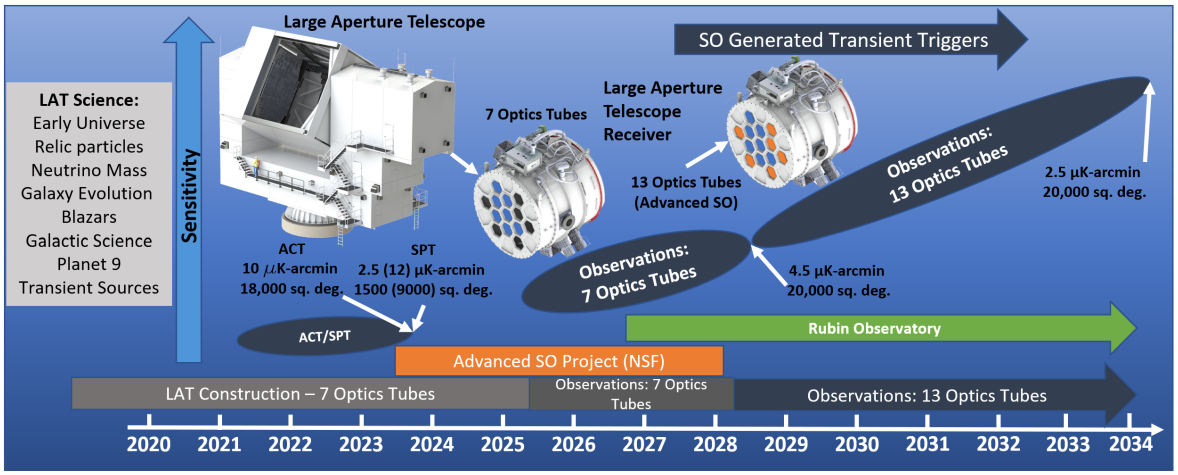

Figure 1. Timeline of the Simons Observatory. The sensitivity, indicated by the overall vertical extent of each ellipse, approximates the survey-science reach of the different programs. The timing of SO and its broad sky coverage are ideally matched to the Rubin Observatory, DESI (2021-26), *Euclid* (launched in July 2023), and *Roman* (due to launch no later than 2027). The 20,000 square degrees of overlapping sky coverage with Rubin is key to achieving the SO science goals. A cutaway of the SO Large Aperture Telescope is shown, along with the Large Aperture Telescope Receiver. The six new optics tubes described in Sec. 2 are represented in orange on the front of the receiver.

Observations with the fully populated receiver will then commence, with a survey planned through 2034. The cumulative survey duration, including both the initial phase and the full-sensitivity phase, is expected to be nine years. Note that the mapping speed of the LATR during the initial SO survey is roughly half that of the instrument during the latter part of the survey, after the upgrade. The forecasts presented in Sec. 3 are based on the cumulative sensitivity of the entire survey with "goal" noise levels, accounting for the sensitivity improvement at the nominal-to-fully-populated LATR transition (see Appendix A for further details). The forecasts presented here include only statistical errors; systematic error contributions will be refined in future, dedicated studies. In addition, *Planck* data are incorporated in all cosmological forecasts unless explicitly stated otherwise — *Planck* is useful for measuring large-scale modes to which SO is less sensitive due to atmospheric noise, particularly in total intensity. As a reference point, the depth of the co-added wide-area SO 93 and 145 GHz maps is expected to reach 2.8 $\mu\mathrm{K}\cdot\mathrm{arcmin}$ at the conclusion of the survey in 2034, assuming the "goal" noise levels in Table 1.[3] Our forecasting approach follows that explained in detail in Ade et al. (2019): we generate simulated sky maps of the microwave sky at all SO and *Planck* frequencies, including all relevant sky components in temperature and polarization (with noise), and then process these through a harmonic-space internal linear combination pipeline to obtain post-component-separation noise power spectra, which are then used in all scientific forecasts. The exceptions to this full-survey-integrated forecasting approach are the time-domain science cases.[4] These include the analysis of AGN light curves in Sec. 3.5, and millimeter-wave transient detection in Sec. 3.10, which both rely on the instantaneous

[3]Including all frequency maps, the depth is expected to reach 2.6 $\mu\mathrm{K}\cdot\mathrm{arcmin}$; the LF and UHF channels are predominantly of use in foreground mitigation, rather than raw CMB sensitivity.

[4]The cosmic birefringence forecast in Sec. 3.3 also does not include *Planck* data.

sensitivity and transient detection pipeline of the SO survey with the fully populated LATR, rather than the cumulative depth of the full nine-year integrated data set.

3 Science goals and forecasts

High-sensitivity, multi-frequency maps of the intensity and polarization of the millimeter-wave sky, observed at a regular cadence, will enable a broad set of new insights into our universe on scales ranging from the surface of last scattering to our Solar System. The deployment timeline and key science forecasts are summarized in Fig. 1 and Table 2, respectively. Fig. 2 gives an overview of the key CMB cosmology observables from the SO LAT survey. Much of the science requires the large sky coverage available from Chile (Fig. 3).

3.1 Constraining the properties of primordial perturbations

By measuring primordial fluctuations in the CMB over twice the range of angular scales probed by the *Planck* satellite, the full SO survey (in combination with *Planck*) will significantly improve characterization of the scale dependence, Gaussianity, and adiabatic nature of the primordial density fluctuations that are the signature of the dynamics of the first moments of the universe (Hanany et al. 2019; Meerburg et al. 2019; Slosar et al. 2019b). SO will halve the current error bar on the scalar perturbation spectral index n_s, testing the near-scale-invariant prediction of inflation over a wider range of scales than accessible to *Planck* (Slosar et al. 2019b). SO will further test early-universe models by constraining the Gaussianity of the perturbations to $\sigma(f_{\rm NL}^{\rm local}) = 1$ via kinematic Sunyaev-Zel'dovich (kSZ) tomography (Münchmeyer et al. 2019; Smith et al. 2018), improving current constraints by a factor of five (Meerburg et al. 2019), and also by constraining primordial isocurvature perturbations.[5] Note that achieving $\sigma(f_{\rm NL}^{\rm local}) = 1$ via kSZ tomography requires overlapping galaxy survey data, as will be available on the SO footprint from Rubin, *Euclid*, and other surveys. Constraints on primordial tensor perturbations, which require data from the SATs, will be described in a separate publication, which will also describe delensing forecasts enabled by the enhanced LAT infrastructure (see Namikawa et al. (2022) and Hertig et al. (2024) for delensing forecasts for the nominal SO survey). Together, these measurements will provide the most detailed constraints to date on the primordial power spectrum and early-universe physics.

3.2 A refined image of the earliest snapshot of the universe

The SO survey of the millimeter-wave sky will provide numerous new insights into fundamental physics. Wide classes of beyond-standard-model (BSM) particle physics scenarios (e.g., some scenarios constructed to solve known theoretical issues like the hierarchy problem; Arkani-Hamed et al. 2016), predict the existence of new light ($\lesssim 1$ eV) species that were in thermal equilibrium at some early time with the primordial plasma (Alexander et al. 2016; Essig et al. 2013; Green et al. 2019; Muñoz et al. 2021). Such scenarios leave distinct imprints in the small-scale damping tail of the CMB temperature and polarization anisotropy power spectra, thus yielding tight CMB-derived constraints on many BSM scenarios, including axions, sterile neutrinos, gravitinos, high-frequency gravitational waves, and other forms

[5] Direct estimates of $f_{\rm NL}^{\rm local}$ from the primary CMB bispectrum will also provide robust bounds, albeit with error bars roughly 2-3 times larger than those expected from kSZ tomography. The primary bispectra will also tightly constrain other shapes of non-Gaussianity (equilateral and orthogonal), with roughly a factor of two improvement over the current bounds from *Planck*.

Table 2. Summary of Enhanced Science Goals from SO LAT Survey[a]

	Current[b]	**SO 2025–2034**	Using Rubin, DESI, or *Euclid*	Reference
Primordial perturbations				
n_s	0.004	0.002	-	Shandera et al. (2019)
$e^{-2\tau}\mathcal{P}(k = 0.2\,\mathrm{Mpc}^{-1})$	3%	0.4%	-	Slosar et al. (2019b)
$f_{\mathrm{NL}}^{\mathrm{local}}$	5	1	✓	Meerburg et al. (2019)
Relativistic species				
N_{eff}	0.2	0.045	-	Green et al. (2019)
Neutrino mass[c]				
$\sum m_\nu$ (eV, $\sigma(\tau) = 0.01$)	0.1	0.03	✓	Dvorkin et al. (2019)
$\sum m_\nu$ (eV, $\sigma(\tau) = 0.002$)		0.015	✓	
Accelerated expansion				
$\sigma_8(z = 1 - 2)$	7%	1%	✓	Slosar et al. (2019a)
Galaxy evolution				
η_{feedback}	50–100%	2%	✓	Battaglia et al. (2019)
p_{nt}	50–100%	4%	✓	Battaglia et al. (2019)
Reionization				
Δz	1.4	0.3	-	Alvarez et al. (2019)
τ	0.007	0.0035	-	Alvarez et al. (2019)
Cluster catalog	4000	33,000	✓	
AGN catalog	2000	96,000	-	
Galactic science				
Molecular cloud B-fields	10s	> 860	-	Hensley et al. (2022)
$\sigma(\beta_{\mathrm{dust}})$	0.02	0.005	-	Hensley et al. (2022)
Solar System Science				
Distance limit for 5 $M_\oplus$ Planet 9	500 AU	900 AU	✓	Fienga et al. (2020)
Asteroid detections		$\sim 10,000$		
Transient detection distance				
Long GRBs, on-axis		1300 Mpc	-	
Low-luminosity GRBs		70–210 Mpc	-	
TDEs, on-axis		670 Mpc	-	

[a] Projected 1σ errors computed with standard methodology as in Ade et al. (2019), scaled to account for the improved noise from the enhanced infrastructure described in Sec. 2 (see Appendix A). Galactic science forecasts are computed as in Hensley et al. (2022). Ade et al. (2019) describes our methods to account for noise properties and foreground uncertainties. We adopt "goal" noise levels for the SO LAT in these forecasts. A 20% end-to-end observation efficiency is used, matching that typically achieved in Chile (as also assumed in Ade et al. 2019). We assume the *Planck* data are included throughout. External data listed in the fourth column are those necessary to achieve the forecasted precision on each individual science target; for the cluster catalog the external data are needed only for obtaining redshifts. Note that the time-domain science forecasts are new to this work, as this topic was not considered in the nominal SO science goals forecasting (Ade et al. 2019).

[b] Primarily from *Planck* (Planck Collaboration et al. 2020b). We anticipate constraints from existing ground-based data to improve on the "current" limits in the near future. These constraints are expected to lie between the "current" and SO levels.

[c] The forecast precision on $\sum m_\nu$ is highly sensitive to the projected error bar on τ, and thus we provide two forecasts here (see Sec. 3.4).

of relativistic energy density in the early universe. SO will either find evidence for new particles via these signatures or constrain BSM theories by improving current limits on the number of relativistic species (Planck Collaboration et al. 2020b) by a factor of four, with $\sigma(N_{\mathrm{eff}}) = 0.045$ (see Fig. 2 and Table 2). For example, the full SO survey will rule out at $> 95\%$ CL any light spin-3/2 particle that was in thermal equilibrium at any time back to re-

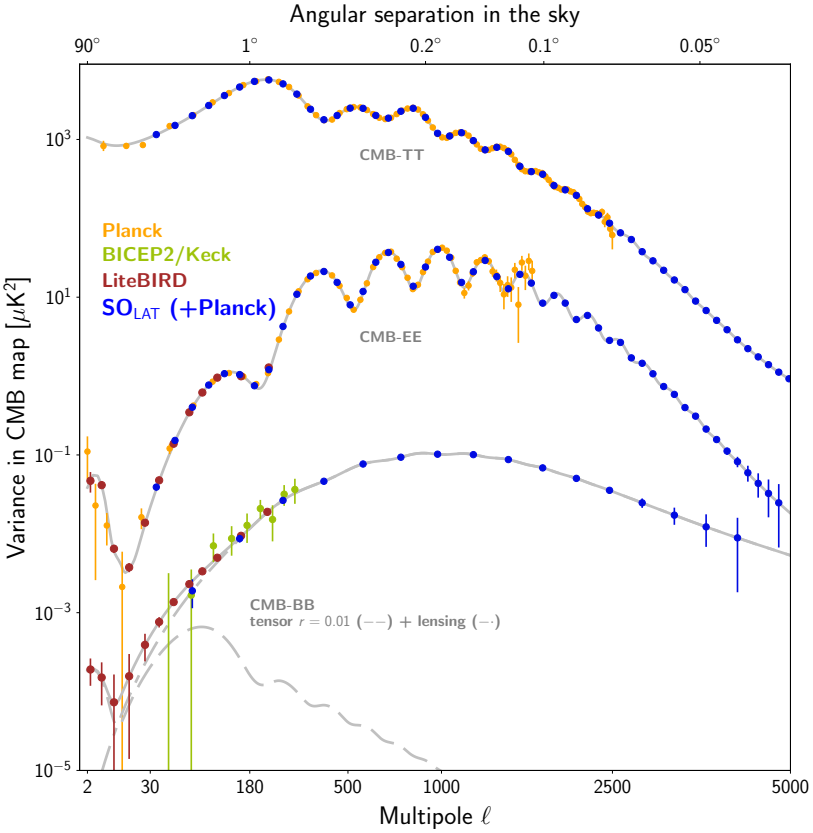

Figure 2. Key CMB cosmology observables that can be derived from the SO LAT sky maps: CMB temperature (TT) and polarization (EE and BB) power spectra. The different colored points with error bars show existing (*Planck* and BICEP2/Keck) and forecast (*LiteBIRD* and SO) power spectrum measurements from various CMB experiments. The forecast SO noise power spectra here include detector and atmospheric noise, as well as the effects of residual foregrounds after component separation, following the methodology described in Ade et al. (2019). *Planck* data are also assumed to be combined with SO, as indicated in the legend. Small-scale power spectrum measurements from existing ground-based CMB experiments (e.g., ACT, SPT, POLARBEAR) are omitted here for clarity.

heating, assuming a standard thermal history of the universe after the particle's decoupling. In particular, SO will significantly improve the precision with which the characteristic phase shift imprinted by free-streaming particles can be detected in the CMB, a unique signature sensitive to BSM physics (Montefalcone et al. 2025). A robust detection of $N_{\rm eff}$ differing from its standard-model value (3.044) would be landmark evidence for new physics, yielding the first direct cosmic signal from the epoch between post-inflationary reheating and neutrino decoupling one second later. Importantly, $N_{\rm eff}$ is a generic, model-independent probe of new light particles in the early universe, thus yielding robust constraints on new physics across a vast search space (Green et al. 2019; Muñoz et al. 2021).

The reported tension between local and cosmological measurements of the rate of expansion of the universe (as characterized by the Hubble constant, H_0; Breuval et al. 2024; Di Valentino et al. 2021a; Freedman et al. 2024; Verde et al. 2019) may be resolved by new particle physics models that can increase the Hubble constant while preserving the fit to current CMB power spectrum data (see, e.g., Di Valentino et al. 2021b, for a review). Mod-

els that alter the pre-recombination dynamics are of particular theoretical interest (Knox & Millea 2020), and generically imprint signatures in the CMB temperature and polarization on small scales. Models that accelerate the recombination process itself are also of interest in this context (e.g., Chiang & Slosar 2018; Schöneberg et al. 2022).[6] The full SO survey data will discriminate among such models (e.g., Galli et al. 2022; Hill et al. 2022; Kou & Lewis 2025; Lynch et al. 2024; Smith et al. 2020), or potentially make a detection. The SO data will also enable sensitive searches for interacting dark matter particles, ultra-light axions, cosmic strings, and primordial magnetic fields, as well as precision tests of Big Bang Nucleosynthesis (Gluscevic et al. 2019; Grin et al. 2019; Grohs et al. 2019).

3.3 Improving constraints on cosmic birefringence

The SO data can be used to search for parity-breaking BSM physics, which can produce cosmic birefringence in the linear polarization of CMB photons (Carroll 1998; Lue et al. 1999). A canonical model generating such an effect is that of a new pseudo-scalar field coupled to the electromagnetic field-strength tensor via a Chern-Simons term (Sikivie 1983; Turner & Widrow 1988). A potential detection of such a field would have profound implications (e.g., Ferreira 2021; Marsh 2016). This cosmic birefringence manifests as a rotation of the plane of linear polarization, giving rise to a nonzero EB power spectrum in the CMB. Strong limits have been placed on the EB polarization angle with ACT data ($0.07 \pm 0.09°$; Choi et al. 2020). Exploiting Galactic foregrounds to break the degeneracy between a miscalibrated instrumental polarization angle and actual cosmological rotation, recent analyses have reported hints of isotropic cosmic birefringence in *Planck* data (Minami & Komatsu 2020), with the latest results estimating a birefringence angle $\beta = 0.342^{\circ}{}^{+0.094^{\circ}}_{-0.091^{\circ}}$ (Eskilt & Komatsu 2022).

The SO LAT survey will observe a significant fraction of the Galactic plane, which will allow us to test this methodology and derive an independent, significantly tighter constraint (Diego-Palazuelos et al. 2022, 2023). Using two detector splits for each of the six LAT frequency channels over the full survey region, and in the multipole range $\ell = 100 - 2000$, the full SO survey will yield $\sigma(\beta) = 0.04°$, more than a factor of two improvement over current error bars, if the methodology and assumptions of Eskilt & Komatsu (2022) are applied to these data. Note that this forecast uses only SO LAT data, i.e., no *Planck* data are included, in contrast to the other cosmological forecasts in this paper.[7] Polarized thermal dust in the Milky Way shows a positive parity-violating TB correlation (Planck Collaboration et al. 2020c; Weiland et al. 2020), limiting current birefringence constraints due to the need to account for this poorly understood, parity-violating foreground; our forecast here assumes this "intrinsic" foreground contribution to the observed EB correlation to be negligible, but this assumption may not hold (Clark et al. 2021). Efforts are ongoing to understand the mechanisms by which dust could produce this parity-violating signal (e.g., Clark et al. 2021; Cukierman et al. 2023; Diego-Palazuelos et al. 2023; Halal et al. 2024; Hervías-Caimapo et al. 2025; Huffenberger et al. 2020; Vacher et al. 2023). SO and complementary surveys (e.g., with the Fred Young Submillimeter Telescope; CCAT-Prime Collaboration et al. 2023) will enable characterization of the dust signal at high resolution and sensitivity, allowing improved modeling and more robust constraints on birefringence. Should a robust EB signal be de-

[6] We note that detailed knowledge of the recombination process is crucial for the interpretation of CMB data (Planck Collaboration et al. 2016a). In this context, the refined recombination codes CosmoRec (Chluba & Thomas 2011) and HyRec (Ali-Haïmoud & Hirata 2011) are designed to reach sufficient accuracy for modeling standard recombination in the analysis of SO data.

[7] Note that $1/f$ noise is included in the SO LAT noise model here, as in all other forecasts.

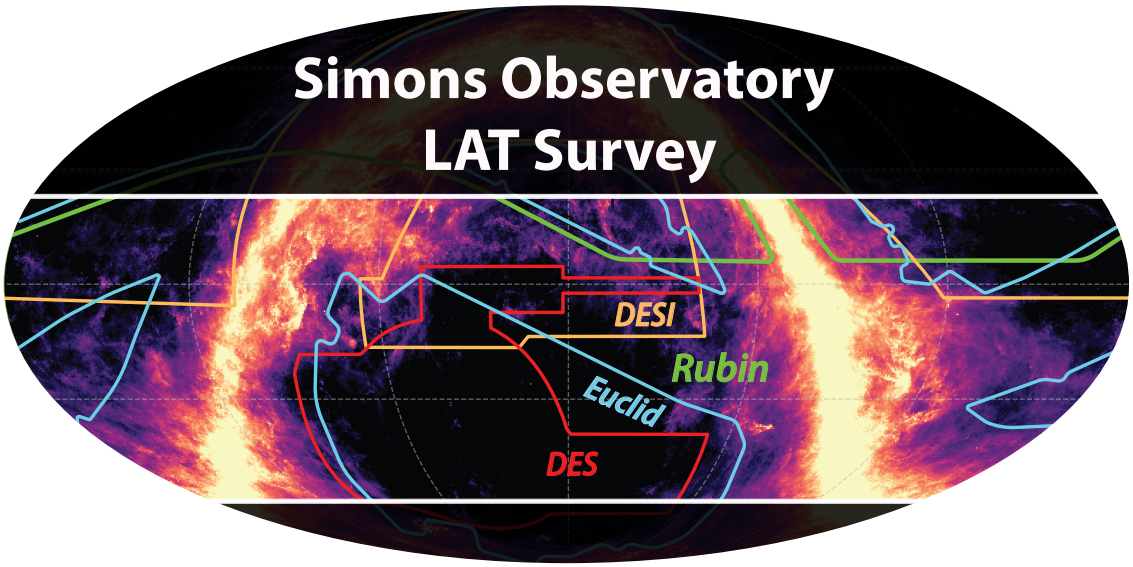

Figure 3. The SO LAT survey (highlighted region with white boundaries) will cover 61% of the sky. This sky coverage overlaps that of the Rubin Observatory and much of DES, DESI, and *Euclid*, as shown. The background image shows the *Planck* 857 GHz total intensity map on a logarithmic scale.

tected with SO, it will be important to account for lensing-induced smoothing of the EB power spectrum in order to derive unbiased constraints on BSM physics (Idicherian Lonappan 2025; Naokawa & Namikawa 2023).

3.4 A new large-scale view of dark matter, baryons, and galaxy clusters

CMB photons interact with matter in the universe as it evolves over cosmic time. Detailed analyses of the deflection of photons due to gravitational lensing from large-scale structures and the scattering of photons from ionized gas in galaxies, groups, and clusters offer exquisite tests of structure formation models and allow constraints on the physical parameters governing these processes, particularly via cross-correlation measurements, as enabled by the SO LAT survey sky coverage shown in Fig. 3. Here we describe a series of science goals that are enabled by measurements of these effects.

Neutrino oscillation experiments show the three neutrino species have a total mass of at least 0.06 eV, or at least 0.1 eV if the hierarchy of particle masses is inverted (Particle Data Group Collaboration 2014). In combination with DESI baryon acoustic oscillation data (Adame et al. 2025), the maps enabled by the enhanced infrastructure described in Sec. 2 will provide a measurement with $\sigma(\sum m_\nu) = 0.03$ eV (Ade et al. 2019). Combined with future improved constraints on the reionization optical depth, τ (e.g., from *LiteBIRD*, Lee et al. 2019), the SO + DESI measurement is expected to improve to $\sigma(\sum m_\nu) = 0.015$ eV.[8] Evidence for non-zero neutrino mass from cosmological data, and the resulting constraints

[8]We also anticipate competitive τ constraints from SO itself via the patchy kinematic Sunyaev-Zel'dovich effect, as explained later in this section; although these will not reach the precision expected from *LiteBIRD*, they will also improve the SO-derived neutrino mass constraint over that obtained with *Planck* constraints on τ. Anticipated improvements on τ from CLASS (Harrington et al. 2016) will also help in this regard.

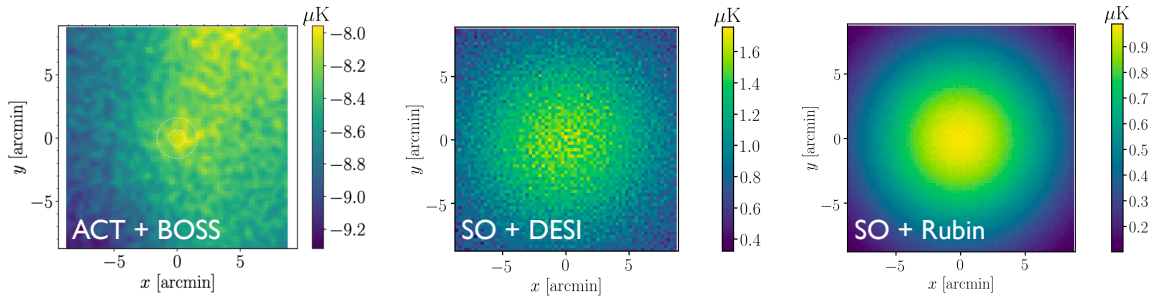

Figure 4. Stacked images of ionized gas density around galaxies measured via the kSZ effect using ACT and BOSS data (left; Schaan et al. 2021), simulated full-SO-survey and DESI data (middle), and simulated full-SO-survey and Rubin data (right). Note that the left image has an overall additive offset and gradient due to residual CMB fluctuations in the stack. The enhanced SO infrastructure will improve the precision of such measurements by nearly two orders of magnitude over current data.

on the hierarchy, will be of significant consequence to particle physics, as detailed in the 2014 and 2023 P5 reports (HEPAP Subcommittee Collaboration 2014, 2023).

The nature of dark energy is one of the most profound questions in modern physics and is a key science target for many ongoing and upcoming wide-area optical surveys, including the Dark Energy Survey (Dark Energy Survey Collaboration et al. 2016), the Hyper Suprime-Cam Survey (Aihara et al. 2022), the Rubin Legacy Survey of Space and Time (LSST Science Collaboration et al. 2009), *Euclid* (Euclid Collaboration et al. 2024; Refregier et al. 2010), *Roman* (Spergel et al. 2015), and others. Precision gravitational lensing measurements of the CMB by the fully populated SO LATR will complement optical observations from Rubin and *Euclid* by extending the redshift range over which we can measure the effects of dark energy to $z > 1$ (Fang et al. 2022). This will probe earlier epochs of cosmic history than accessible to optical telescopes, which are limited by the faintness of distant galaxies, and will enable novel tests of modified gravity theories (Slosar et al. 2019a). Concretely, we forecast a 1% constraint on the amplitude of the matter power spectrum at $z = 1 - 2$ via the combination of SO CMB lensing maps with galaxy catalogs from Rubin and *Euclid*, through combined analyses of CMB lensing auto- and cross-power spectra with these surveys. These constraints will precisely probe dark energy at the epoch when its dynamical influence first becomes evident. In addition, tomographic measurements of the growth of structure over a wide redshift range (out to $z \approx 3$ and perhaps beyond; Qu et al. 2023; Schmittfull & Seljak 2018) will also be enabled by similar cross-correlations with these and other surveys, including *Roman* and *SPHEREx* (Doré et al. 2014).

Characterizing the energy efficiency of feedback in galaxies, sourced by supernovae and active galactic nuclei, is a major focus of galaxy evolution studies. Feedback is also the dominant physical uncertainty in optical gravitational lensing analyses that seek to constrain dark energy. Combined with measurements of large-scale structure from DESI, Rubin, and *Euclid*, the SO maps of integrated electron pressure (Compton-y) and momentum from the thermal and kinematic Sunyaev-Zel'dovich (SZ) effects (Sunyaev & Zeldovich 1980, 1972; Zeldovich & Sunyaev 1969) will uniquely measure the baryon content in galaxies, groups, and clusters – a quantity not measurable with optical telescopes – and will constrain the feedback efficiency to the few percent level. Fig. 4 shows simulated stacked images of the ionized gas

density in the circumgalactic medium around DESI and Rubin galaxies,[9] as measured using the kSZ effect with the full SO survey data. These measurements will improve over the precision of recent data from ACT and BOSS (Schaan et al. 2021, also shown in Fig. 4) by nearly two orders of magnitude (Battaglia et al. 2017) (see also, e.g., Hadzhiyska et al. (2024) for recent kSZ measurements using ACT and DESI and Bleem et al. (2022); Chandran et al. (2023); Coulton et al. (2024a); McCarthy & Hill (2024); Planck Collaboration et al. (2016b); Tanimura et al. (2022) for state-of-the-art Compton-y maps from ACT, SPT, and *Planck* data).

The SO maps will complement 21-centimeter experiments that probe the epoch of reionization (e.g., HERA Collaboration et al. 2023; Mellema et al. 2013; Tingay et al. 2013) by distinguishing among different models for how the universe was heated by the first ionizing sources. The "patchy" kSZ signal imprinted in the CMB during this epoch, due to scattering off the newly freed electrons, will enable the duration of the epoch of reionization to be measured with an uncertainty of $\sigma(\Delta z) = 0.3$ (about 60 million years; Alvarez et al. 2019). This signal, interpreted using astrophysical reionization modeling, will also allow a determination of the optical depth τ, independent of large-scale CMB E-mode measurements (Alvarez et al. 2021). We forecast that SO can reach $\sigma(\tau) = 0.0035$ using this new method, which relies on a joint analysis of the kSZ 2- and 4-point functions (Alvarez et al. 2021; Ferraro & Smith 2018).[10] This forecast is within a factor of two of the cosmic-variance-limited error bar from the large-scale E-mode polarization targeted by satellite missions such as *LiteBIRD* (LiteBIRD Collaboration et al. 2023).

Using the unique redshift independence of the thermal SZ (tSZ) effect, SO will extend tSZ cluster detection into the epoch in which the first massive, virialized structures formed at $z \gtrsim 2$. Thermal SZ surveys from ACT, SPT, and *Planck* have led the field in constructing clean, complete, nearly mass-selected cluster samples, with the latest catalogs comprising several thousand galaxy clusters in total (Hilton et al. 2021; Planck Collaboration 2016; SPT, DES Collaboration 2024). We forecast that the full SO survey will detect 33,000 clusters, with redshifts from overlapping DESI, Rubin, *Euclid*, and *SPHEREx* data, as well as dedicated optical and near-IR observations. This forecast uses the multifrequency matched-filter methodology described in Madhavacheril et al. (2017) (following Herranz et al. 2002; Melin et al. 2006) assuming the gas pressure profile from Arnaud et al. (2010)[11] with a cut on SNR > 5 used to define the cluster sample. SO will thus provide the community with a homogeneous, well-defined catalog for follow-up studies out to high redshifts, with ≈ 200 clusters in the unique $z > 2$ discovery space (Mantz et al. 2019), enabling a broad range of multiwavelength science, including X-ray analyses with *eROSITA* (Merloni et al. 2024). Mass estimates will be enabled by galaxy weak lensing data from Rubin and *Euclid* for clusters at $z \lesssim 1$ and by SO's own CMB lensing data at higher redshifts. SO measurements of high-z clusters and proto-clusters will also provide crucial total flux constraints for high-resolution follow-up observations with interferometric facilities (e.g., Kitayama et al. (2023); van Marrewijk et al. (2024)).

In addition, the six frequency channels of the SO LATR will enable measurement of

[9] For DESI, we assume 2.9 million luminous red galaxies in this stack, measured on an overlapping sky area of 10,000 deg^2; for Rubin, we assume 1.5 billion galaxies measured on 16,000 deg^2.

[10] For the purposes of this forecast, foregrounds are treated as Gaussian; future work will refine this methodology (MacCrann et al. 2024; Raghunathan et al. 2024).

[11] The exact pressure profile parameters used are: $P_0 = 8.403$, $c = 1.156$, $\alpha = 1.062$, $\gamma = 0.3292$, and $\beta = 5.4807$, with a hydrostatic mass bias $1 - b = 0.8$ used to set the normalization of the pressure–mass relation.

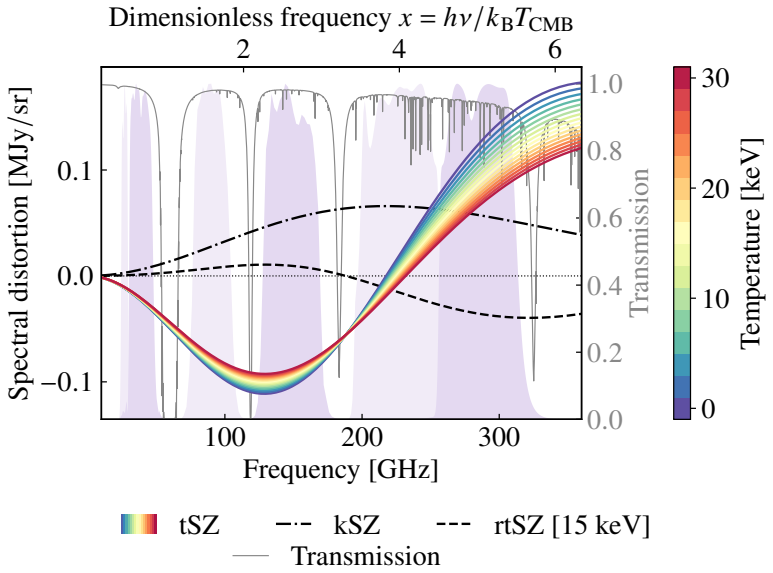

Figure 5. Spectral dependence of the intensity of the kinematic SZ (dot-dashed curve) and relativistically corrected thermal SZ effects, where the line color denotes the electron temperature as labeled. The relativistic corrections are computed using `SZpack` (Chluba et al. 2012; Lee & Chluba 2024), with the difference between the thermal SZ spectrum for a 15 keV plasma versus that for the non-relativistic case shown as a dashed curve. The background shaded purple regions show the six bands of the SO LATR (Sierra et al. 2025; Simon et al. 2018; Walker et al. 2020), and the light gray curve, computed using the `am` code (Paine 2019), shows the atmospheric transmission for median conditions at the SO site.

the relativistic tSZ (rtSZ) effect, particularly for massive clusters, building upon the recent 3.5σ detection from ACT (Coulton et al. 2024b) (see also earlier $\approx 2\sigma$ hints using *Planck* data in Erler et al. 2018; Remazeilles & Chluba 2024). Example rtSZ spectra computed with `SZpack` (Chluba et al. 2012; Lee & Chluba 2024) are shown in Fig. 5, along with the kSZ spectrum, the SO LATR bands (Zhu et al. 2021), and the atmospheric transmission at the SO site. The spectra in the plot are computed for an example cluster with Compton-y parameter $y = 10^{-4}$, optical depth $\tau = 0.01$, and line-of-sight peculiar velocity $v_{\rm LOS}/c = 0.005$. Relativistic tSZ measurements will yield simultaneous inference of the electron pressure and temperature (and hence density) in massive halos, thereby allowing new approaches to cluster mass estimation and novel constraints on intracluster medium physics, particularly in combination with X-ray data (see, e.g., Mroczkowski et al. 2019, for a review).

3.5 A wealth of extragalactic sources: time-variable blazars and dusty galaxies

Recent measurements of extragalactic source counts from ACT and SPT (Everett et al. 2020; Gralla et al. 2020; Vargas et al. 2023) are broadly consistent with AGN and dusty star-forming galaxy (DSFG) models, including the Lagache et al. (2020) AGN and Cai et al. (2013) DSFG models, at SO frequencies between 93 and 280 GHz. These models, combined with the noise levels in Table 3, indicate that 93 GHz will be the most sensitive frequency for detecting AGN, with an expected count of approximately 96,000 at the goal sensitivity (see Appendix A for more details on the sensitivity estimation). The 5σ source sensitivity with a matched-filter source finder is 2.0 mJy over a sky fraction of 0.52. This sky fraction

Frequency [GHz]	Single Observation Sensitivity [mJy]		Co-added Sensitivity [mJy]	
	Baseline	Goal	Baseline	Goal
27	37	27	2.8	2.3
39	25	19	1.8	1.5
93	9.5	6.9	0.52	0.40
145	13	8.3	0.67	0.50
225	26	17	1.4	0.98
280	49	34	2.5	1.8

Table 3. Sensitivity of the fully populated LATR to point sources, specified as 1σ root-mean-square (RMS) noise. The single observation sensitivities are relevant for transient detections and the co-added sensitivities correspond to those obtained by the end of the survey. For each we report baseline and goal sensitivities.

corresponds to the SO LAT survey region, excluding the Galactic plane based on the 80% sky fraction *Planck* Galactic emission mask.

The most sensitive bands to detect DSFGs will be 225 and 280 GHz. If we consider the baseline noise from Table 3, since high-frequency channels are prone to high atmospheric loading, the 5σ detection cut is around 7.0 and 12.5 mJy for 225 and 280 GHz, respectively. Considering a sky fraction of 0.52 and the Cai et al. 2013 dusty models, we expect to detect around 32,000 and 36,000 DSFGs in each respective band. Both frequencies will yield a similar number of detections at the baseline noise, and both flux measurements help to constrain the spectral energy distribution of these galaxies. Combining these data with far-infrared measurements enables constraints on the physical properties of DSFGs, including redshift, temperature, emissivity, and luminosity (Bendo et al. 2023; Reuter et al. 2020; Su et al. 2017). SO will detect DSFGs up to redshifts $z = 4$, and strongly lensed ones beyond $z = 6$, some with magnifications of several tens. The latter make promising follow-up targets for the Atacama Large Millimeter Array (ALMA), to resolve compact, young galaxies in their early evolutionary phases (Spilker et al. 2016).

In Fig. 6 we show the estimated number of AGN and DSFGs that we expect to detect given baseline or goal sensitivities. We note that the predicted number of DSFG detections varies by a factor of ~ 4 between baseline and goal sensitivities. These forecasts are based on the best available models for the number of sources at different flux limits, but the low-flux regime is currently poorly constrained. SO data will refine these models and improve our understanding of AGN and DSFG populations as a whole.

For the source sensitivities in Table 3, backgrounds constitute a significant contribution to the total noise in all bands. At long wavelengths the relevant background is the CMB, but at shorter wavelengths the CIB is dominant. The possibility thus arises that deeper observations, reaching sensitivities below the CIB confusion limit, could be undertaken in sub-regions of the LAT survey, which would allow techniques such as probability of deflection approaches (P(D); e.g., Glenn et al. 2010) to set constraints on the CIB population beyond the confusion limit.

Most of the bright AGN found at millimeter frequencies are blazars. Blazars are AGN with relativistic jets aligned with the line of sight, often appearing variable. SO will increase the *Planck* catalog of AGN (Planck Collaboration et al. 2016c) by a factor of ~ 50, and will provide regularly sampled light curves. For instance, the goal daily sensitivity at 93 GHz of

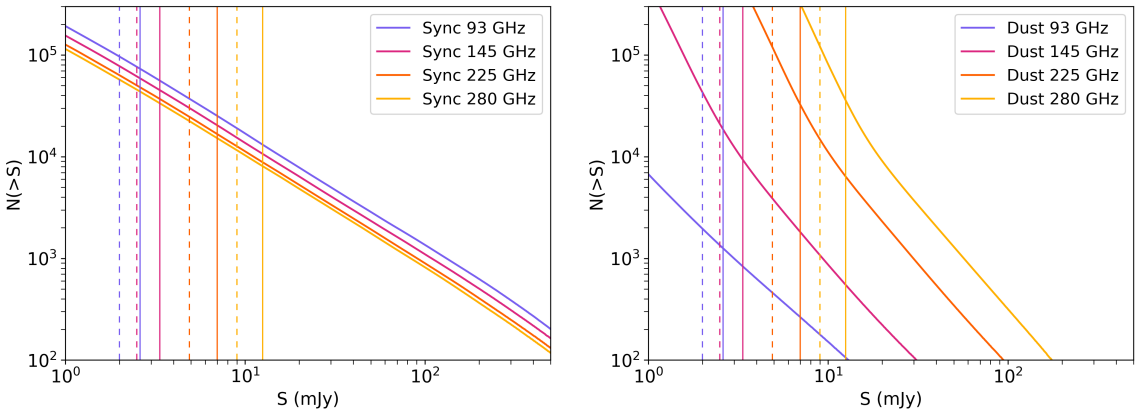

Figure 6. Total number of sources above different flux limits S, as a function of S in mJy, assuming a sky fraction of 0.52. Left: models for AGN synchrotron emission at four frequencies (Lagache et al. 2020). Right: model dust emission for DSFGs (Cai et al. 2013) at the same four frequencies. Vertical lines indicate the 5σ sensitivity for the SO baseline (solid) and goal (dashed) sensitivities.

6.9 mJy (Table 3) translates to 3σ daily measurements of 21 mJy sources. According to the AGN model of Lagache et al. (2020), this implies that SO can provide light curves for 7,500 AGN at its regular observing cadence, expected to be every day or two when a source is in the field. (Each source will be unobservable for about a month out of each year, when it is too close to the Sun.) Combining multiple observations will increase the available number of light curves. For instance, averaging six observations would enable light curves of $\sim 20,000$ AGN at the mean 3σ level.

This monitoring program will be a great improvement over the state of the art (Bonato et al. 2019; Cortes et al. 2024; Lister et al. 2018; Richards et al. 2011), and will enable study of the innermost portions of the jets, which are opaque at longer wavelengths. Aside from measuring flaring events and stochastic variability, these data can be used to search for supermassive black hole binaries (SMBHBs) which are expected to have sinusoidal light curves. Kiehlmann et al. (2024) estimate that about 1% of the radio blazar population are SMBHBs. Hence, we expect to find $\mathcal{O}(100)$ SMBHBs with the monitoring program.

AGN light curves will be also valuable for cross-correlations with other tracers, including neutrino observatory measurements (e.g., IceCube Collaboration et al. 2018). The blazar SED has two bumps. The low-energy bump (Urry 1998), spanning the radio to UV, peaks in the millimeter and is due to synchrotron emission from ultra-relativistic electrons. The emission mechanism behind the high-energy bump, which spans the UV to gamma-ray portion of the electromagnetic spectrum, is still under debate. Its origin is either leptonic, inverse-Compton scattering of lower energy photons (Dermer & Schlickeiser 1993; Maraschi et al. 1992), or hadronic, proton-synchrotron radiation or photo-pion production (Dermer & Atoyan 2001; Mücke & Protheroe 2001). Cross-correlating blazar light curves over a range of wavelengths can elucidate the physical processes that shape and change blazar SEDs. Many studies have compared radio, optical, and gamma-ray blazar light curves (e.g., Liodakis et al. 2018; Rani et al. 2013). However, few of these studies have included millimeter-wavelength light curves (e.g., Hood et al. 2023), even though millimeter-wavelength emission is a strong indicator of synchrotron radiation.

3.6 Insights into the polarized Galactic interstellar medium

Arcminute-resolution millimeter-wave maps of the SO footprint, which includes much of the Galactic plane, will be valuable for answering many questions about the physical mechanisms responsible for polarized Galactic emission, via measurements of the dust and synchrotron spectral energy distributions across the sky, and detections or upper limits on polarized CO line emission and anomalous microwave emission (AME; Hensley et al. 2022). SO will detect AME polarization if the AME is polarized at the $\gtrsim 0.1\%$ level, which is sufficient to distinguish between competing theories of ultrasmall grain alignment (Hensley et al. 2022), such as resonance paramagnetic alignment (Hoang et al. 2013; Lazarian & Draine 2000), or suppression of alignment due to quantum mechanical effects (Draine & Hensley 2016). Additionally, SO will determine what fraction of the AME could be contributed by magnetic dipole emission from ferromagnetic grains, which are distinguished by their unique polarization signature (Draine & Hensley 2013). See Dickinson et al. (2018) for a recent review. Together with large-area starlight polarization surveys such as PASIPHAE (Tassis et al. 2018), these data will yield new insights into the physics of Galactic emission and the multi-scale structure of the magnetized interstellar medium (Fissel et al. 2019; Hensley et al. 2019).

Recent ACT observations of the Galactic center (Fig. 7; Guan et al. 2021) offer a glimpse of the physical processes probed at SO frequencies, which will complement multiwavelength observations (e.g., Butterfield et al. 2024; Heywood et al. 2019). As detailed in Hensley et al. (2022), SO will resolve the magnetic field structure of more than 860 molecular clouds with 1 pc resolution and at least 50 independent, high-SNR polarization measurements per cloud, compared to *Planck*'s sample of tens of clouds. Additionally, SO will be able to detect polarized dust emission in 400 Galactic cold clumps, prime candidates in the formation and evolution of stellar cores. This is a factor of 200 greater than *Planck*, and will enable detailed statistical studies on their magnetic field structure and role in stellar formation (Clancy et al. 2023). In the more diffuse ISM, the SO dust polarization maps can be used in conjunction with ISM emission tracers to quantitatively study the small-scale structure of polarized emission (e.g., Clark & Hensley 2019; Clark et al. 2015; Córdova Rosado et al. 2024) and to probe the magnetic field structure in diffuse media (Lei & Clark 2024).

Component separation techniques and detector passband variation can be exploited to build maps of velocity-integrated CO line emission from continuum data (Planck Collaboration et al. 2014). Hensley et al. (2022) forecast that SO will detect or constrain polarization of the CO(2–1) line at sub-percent levels in dense molecular clouds, including Ophiuchus and Orion. CO line polarization via the Goldreich-Kylafis effect probes the magnetic field strength and orientation in molecular clouds (Crutcher 2012; Goldreich & Kylafis 1981).

3.7 The composition of interstellar dust

Classical models of the composition of interstellar dust posit two classes of dust: predominantly silicate and predominantly carbonaceous. These models predict a strong divergence of the dust total intensity and polarization spectra – i.e., a wavelength-dependent polarization fraction – in the frequency range probed by SO. However, analyses of data from *Planck* and the Balloon-borne Large Aperture Submillimeter Telescope for Polarimetry (BLASTPol) find that the difference in spectral indices between dust total intensity and polarization at ∼submillimeter wavelengths is only on the order of a few percent at most (Ashton et al. 2018; Planck Collaboration et al. 2020c; Shariff et al. 2019). This lack of evidence for the predicted divergence is driving new theoretical work on dust composition (Draine & Hensley 2021a;

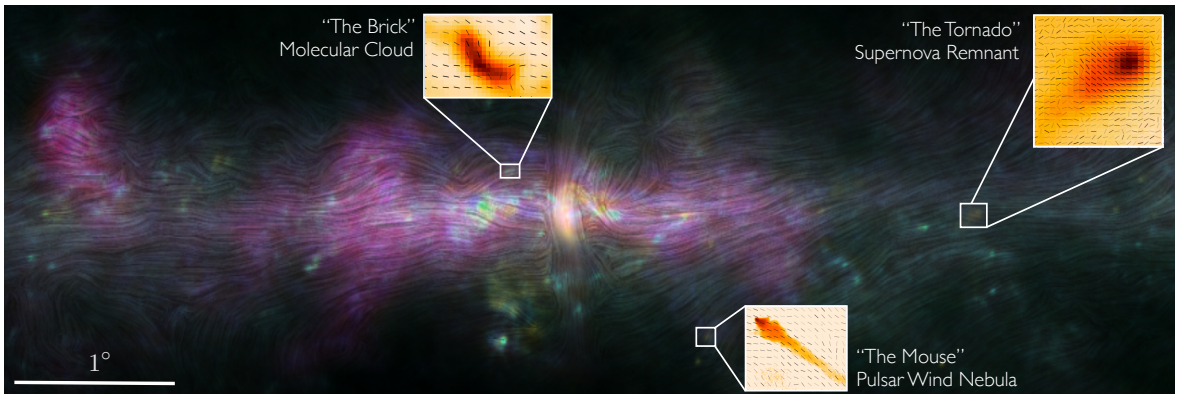

Figure 7. The ACT view of the Galactic Center and zoom-ins to particular regions (adapted from Guan et al. 2021). The three-color background image comprises ACT 90 GHz (red), 150 GHz (green), and 220 GHz (blue) observations coadded with *Planck* data at similar frequencies. Overlaid magnetic field orientation is from ACT 90 GHz polarization. The SO frequency coverage spans synchrotron-dominated (more red) to dust-dominated (more blue) emission, enabling a uniquely comprehensive view of the magnetic field morphology. Insets illustrate particular regions of interest. "The Brick" Molecular cloud: *Herschel* total intensity overlaid with ACT 220 GHz magnetic field orientation data. "The Tornado" supernova remnant: ACT 90 GHz intensity and magnetic field orientation data. "The Mouse," a pulsar wind nebula: MeerKAT 1.28 GHz total intensity (Heywood et al. 2019) and ACT 90 GHz magnetic field orientation.

Guillet et al. 2018; Hensley & Draine 2023; Ysard et al. 2024). SO will test these models, including constraining $\beta_{\rm dust}$, the spectral index of the modified blackbody SED characteristic of polarized dust emission. Using sky models from the Python Sky Model (Thorne et al. 2017), we forecast that SO measurements combined with *Planck* and *Wilkinson Microwave Anisotropy Probe* (*WMAP*) data will measure $\beta_{\rm dust}$ to $\sigma(\beta_{\rm dust}) = 0.005$, sufficient to test the two-component dust model (Hensley et al. 2019). Constraints on $\beta_{\rm dust}$ within smaller regions enable tests of recent evidence for variability of the dust spectral index (Ade et al. 2025) and of the dust SED more generally (Pelgrims et al. 2021; Ritacco et al. 2023). The evidence for $\beta_{\rm dust}$ variability can also be investigated in cross-correlation with filamentary ISM structures in neutral hydrogen (Ade et al. 2023).

Testing this paradigm will constrain the degree of dust homogenization via interstellar medium (ISM) processing, the rate of dust production in stars, and the composition of the grains that coagulate into solid bodies in protoplanetary disks (Dartois et al. 2024; Hensley et al. 2019; Hensley & Draine 2023). SO data can also be compared with optical starlight polarization measurements, including from PASIPHAE (Tassis et al. 2018). The ratio of far infrared to optical polarization constrains the shape, porosity, and composition of interstellar grains (Draine & Hensley 2021b; Guillet et al. 2018; Planck Collaboration et al. 2020d).

3.8 Solar system bodies and exo-Oort clouds

Reflected sunlight from objects falls off rapidly with distance from the Sun, so the strongest limits on massive outer Solar System objects come from their intrinsic thermal emission. The strongest bounds on unknown giant planets are set by the *Wide-field Infrared Survey Explorer* (*WISE*), excluding planets more massive than Saturn closer than 28,000 AU (Luhman 2014). The spectra of smaller, faster-cooling planets peak at longer wavelengths, well suited for

millimeter observations (see Naess et al. (2021a) for details on the model assumed here). A 5 $M_\oplus$ Planet 9 can be detected with SO, at distances ranging from 500 AU in the more shallowly observed regions over half the sky, to 900 AU over large parts of the sky. For a 5 $M_\oplus$ Planet 9, a search with ACT data ruled out 17% of the orbital parameter space (Naess et al. 2021a), and planetary ephemerides data have been used to exclude such an object within 500 AU (Fienga et al. 2020).

The Solar System is thought to be surrounded by a large, roughly spherical shell of rock and dust known as the Oort cloud (Oort 1950). Our own Oort cloud has never been directly observed, but SO may be able to detect similar structures around other stars, i.e., exo-Oort clouds. Hensley et al. (2022) forecast the pre-upgraded-LATR SO sensitivity to exo-Oort clouds at 280 GHz using simulated dust emission and Oort cloud emission profiles (Baxter et al. 2018) placed around *Gaia* stars within 70 pc (see also Nibauer et al. 2020, 2021). SO will detect (at $\sim 3\sigma$) exo-Oort clouds if their occurrence rate is similar to the detection rate of giant planets (Fernandes et al. 2019; Wittenmyer et al. 2020, $f_{\rm Oort} = 0.3$). As elaborated in Hensley et al. (2022), SO will also probe debris disks from exoplanet formation around nearby stars, constraining the statistical properties of the debris disk population and prioritizing candidates for higher-resolution follow-up with ALMA (e.g., MacGregor et al. 2017; Nederlander et al. 2021).

3.9 Asteroid regoliths

The composition and dynamics of asteroids provide an important window into the composition of the early solar system (e.g., Michel et al. 2015). Observations of asteroids at millimeter wavelengths have shown a consistent deficit in flux as compared to expectations from the infrared (e.g., Johnston et al. 1982; Webster et al. 1988). Since the unconsolidated surface, or regolith, of the asteroid is partially transparent in the millimeter, this millimeter flux deficit is connected to the composition of the regolith, which is otherwise difficult to ascertain. Historically this drop in flux has been interpreted as a change in effective emissivity due to regolith grain size or packing (Redman et al. 1992). However, more recent, comprehensive analysis has suggested the origin may lie instead in steep temperature gradients of several K/centimeter lying just below the surface (Keihm et al. 2013).

Until recently, astronomers have been limited to targeted millimeter observations of asteroids. With the new generation of CMB experiments, however, it has become possible to make catalogs of asteroid flux in the millimeter. SPT made the first detection of three asteroids using a ground-based CMB telescope (Chichura et al. 2022), while ACT published the first extensive catalog of 170 asteroids (Orlowski-Scherer et al. 2024). Both experiments found a systematic flux deficit in the millimeter, with Orlowski-Scherer et al. (2024) finding a spectral shape to the deficit wherein the deficit was more severe at 150 and 220 GHz than at 90 GHz.

While the precise distribution of asteroid fluxes in the millimeter/sub-millimeter is currently unknown, to first order it will likely follow the size distribution, which is well described by a power law with $\alpha = -2.5$. Accounting for the r^2 scaling of the flux with asteroid radius, this leads to a $dN \propto F^{-1.25}$ scaling for dN the number density of asteroids and F the flux. Assuming this, we conservatively estimate that SO will detect approximately 100 times more than the Orlowski-Scherer et al. (2024) sample, on the order of ten thousand asteroids. We further expect the detection of the largest trans-Neptunian objects (TNOs). We scale the

total S/N of a number of asteroids by

$$x_{\rm Earth}^{-2} x_{\rm Sun}^{-1/2} x_{\rm diameter}^{2} x_{\rm S/N}$$

where $x_{\rm earth}$ is the ratio of the Earth-centered TNO distance to Earth-centered asteroid distance, $x_{\rm Sun}$ is the same for the Sun-centered distance, $x_{\rm diameter}$ is the ratio of their physical diameters, and $x_{\rm S/N}$ is the projected SO/ACT S/N ratio. The exponents account for the scaling of the flux with the various parameters in the Rayleigh-Jeans limit of the Standard Thermal Model (Lebofsky et al. 1986). Distances for the TNOs are evaluated January 1, 2025, and will not meaningfully change over the SO lifetime. What is not accounted for here is the emissivity of the TNO; performing this scaling for several asteroids helps marginalize over this uncertainty. We should detect a number of the largest TNOs, specifically (50000) Quaoar, (136472) Makemake, (136108) Haumea and (134340) Pluto at $\geq 5\sigma$ each. Other, larger TNOs have projected S/N $\simeq 1-3\sigma$, indicating that stacking analyses may also be fruitful.

3.10 The unexplored millimeter transient sky

The study of transient astronomical signals at millimeter wavelengths is opening a new frontier in astrophysics. Typically, the millimeter emission is synchrotron radiation produced by particles accelerated as a shock plows into an ambient medium. For decades, observations at centimeter wavelengths have been used to study the explosion and environment properties of explosive phenomena such as supernovae (SNe; e.g., Weiler et al. 2002), gamma-ray bursts (GRBs; e.g., Chandra & Frail 2012), tidal disruption events (TDEs; e.g., Alexander et al. 2020), and novae (e.g., Chomiuk et al. 2021). By contrast, the millimeter regime remains largely unexplored.

Recent years have seen new opportunities for millimeter time-domain astronomy. One reason is that the discovery of young ($\lesssim$ days-old) transients by optical surveys has become routine, enabling fast turnaround follow-up observations using sensitive millimeter interferometers (Andreoni et al. 2022; Berger et al. 2023; Ho et al. 2019; Maeda et al. 2021). In addition, transients have been discovered blindly at millimeter wavelengths for the first time, in CMB survey data (Biermann et al. 2024; Guns et al. 2021; Li et al. 2023; Naess et al. 2021a; Whitehorn et al. 2016), and these data have also been used to put millimeter-wavelength flux limits on known extragalactic transients (Hervías-Caimapo et al. 2024).

With SO, transient events will be routinely and efficiently discovered directly in the millimeter, allowing for follow-up observations by the transient community. The SO rapid transient analysis pipeline will generate daily maps for transient detection and discovery, as well as light curves for each identified transient source to be released to the community within 30 hours. We will release light curves with a typical cadence of about one day, and a time resolution of order minutes. In addition, more slowly evolving faint transients can be detected in stacked maps.

One class of extragalactic transients of interest are interacting supernovae, i.e., core-collapse supernovae exploding in dense circumstellar material. Growing evidence suggests that some massive stars shed a significant fraction of their mass in the final stages of their lives (Smith 2014), perhaps due to vigorous convection in the late stages of nuclear burning (Quataert & Shiode 2012; Shiode & Quataert 2014) or binary interaction (e.g., common-envelope evolution; Chevalier 2012). Enhanced mass loss on timescales of days to years would leave dense material close to the star (6–600 AU). When the star explodes, this circumstellar

material can be detected by its luminous millimeter-wave emission (Maeda et al. 2023, 2021; Yurk et al. 2022).

Another important class of extragalactic transients is long-duration GRBs (LGRBs), produced in the powerful jets launched by collapsing massive stars (Piran 2004). A long-standing question in the GRB field is whether long-duration GRBs are a rare and distinct endpoint of stellar evolution, or the extremum of a broad continuum of relativistic stellar explosions (e.g., Cano et al. 2017). SO could address this question by: (i) measuring the beaming fraction through the detection of off-axis events; (ii) finding events that bridge the gap between GRBs and ordinary supernovae, such as low-luminosity GRBs (LLGRBs; Bromberg et al. 2011; Cobb et al. 2006; Liang et al. 2007; Nakar 2015), which are a potential site of high-energy neutrinos (Murase et al. 2008) and cosmic rays (Zhang et al. 2018); and (iii) looking for "dirty fireballs" (Dermer et al. 1999), i.e., jets with lower initial Lorentz factors than classical GRBs. Inferring the initial Lorentz factor of a jet requires disentangling the forward and reverse shock components of the afterglow, which is most readily done using millimeter observations (Laskar et al. 2018, 2019; Perley et al. 2014).

GRB reverse shocks are predicted to be the most frequent class of extragalactic transients detected by SO (Eftekhari et al. 2022; Table 4). GRB reverse shocks are an emission component from shock propagation through the ejecta as the GRB jet collides with the interstellar medium. The reverse shock thus probes the physical properties of the GRB outflow (Nakar & Piran 2004). SO has the potential to conduct the most sensitive, unbiased survey of millimeter-wave reverse-shock emission over half the sky.

Relativistic jets launched in tidal disruption events, when a star is pulled apart by a supermassive black hole, can be luminous millimeter transients early in the event (Andreoni et al. 2022; Zauderer et al. 2011). The fraction of TDEs harboring relativistic outflows appears to be small (Alexander et al. 2020). SO blind millimeter-wave surveys will help to independently measure the event rate. In addition, millimeter observations are sensitive to outflows with lower energies than centimeter-wavelength observations (Alexander et al. 2020).

SO transient observations could also probe the physics of shock acceleration. In the framework typically applied to model supernova centimeter-wave observations, the electrons are presumed to be accelerated into a power-law energy distribution (e.g., Chevalier 1998). Interestingly, millimeter observations of fast blue optical transients (FBOTs) such as AT2018cow (Prentice et al. 2018) and AT2020xnd (Perley et al. 2021) show evidence for a separate emission component at millimeter wavelengths (100–200 GHz) that does not fit the standard model used to describe the late-time low-frequency (< 40 GHz) data (Ho et al. 2019, 2022; Margutti et al. 2019). One possibility for the origin of the millimeter component is a Maxwellian distribution of electrons, i.e., electrons that are not accelerated into a power-law distribution (Margalit & Quataert 2021, 2024).

SO will constrain the intrinsic rates of extragalactic millimeter transients, which are now quite theoretically uncertain for many classes of transients (Eftekhari et al. 2022). We forecast the distance that SO can probe for several key classes of extragalactic transients in Table 2, with further forecasts in Table 4. For most classes, this calculation simply depends on the luminosity of the source and the sensitivity of our observations. We estimate a baseline single-observation rms sensitivity of $\sim$13 mJy at 145 GHz, and use this in our forecasts, assuming a 6σ threshold for extragalactic transient detection. We further forecast detection rates for each class of transients from current volumetric rate estimates and the SO detection distance, assuming that SO will discover transients over 52% of the sky (the SO LAT survey

Class	Volumetric Rate ($\mathrm{yr}^{-1}\mathrm{Mpc}^{-3}$)	L_ν ($\mathrm{erg\,s}^{-1}\,\mathrm{Hz}^{-1}$)	Distance (Mpc)	Detection Rate (yr^{-1})
Extragalactic fast (1–10 d duration)	–	–	–	< 10
Long-duration GRB, on-axis	4×10^{-10}	10^{32}	1300	2
Long-duration GRB, off-axis	6×10^{-9}	3×10^{30}	360	0.6
TDE, on-axis	3×10^{-11}	10^{31}	670	0.02
Low-luminosity GRB	2×10^{-7}	10^{29}–10^{30}	70–210	0.1–4
AT2018cow-like FBOT	10^{-7}	10^{30}	210	2
Interacting SN	10^{-8}	10^{27}–10^{30}	< 210	$\lesssim 0.2$
Stellar flares	–	–	–	180

Table 4. Estimated detection rates by SO for different classes of extragalactic transients at 145 GHz, and for stellar flares at 90 GHz. We define off-axis long-duration GRBs to have $\theta_{\rm obs} = 0.4$. For transients lasting a few days (extragalactic fast and long-duration GRB on-axis) we use a goal sensitivity of 13 mJy rms in a single observation and require a 6σ detection. Other events have a longer duration, so we use a baseline sensitivity of 4.9 mJy from one-week stacks and again require a 6σ detection. Stacking maps would increase the sensitivity for longer-lived events. SO observations will constrain the significant theoretical uncertainty on the intrinsic rates of these transients. The detection rate of fast extragalactic transients is taken from systematic searches in SPT data (Guns et al. in prep). The detection rate of stellar flares is extrapolated from recent ACT and SPT detections rate (Biermann et al. 2024; Li et al. 2023; Tandoi et al. 2024) to the SO goal sensitivity and sky coverage, requiring 5σ detections.

footprint with the *Planck* 80% sky fraction Galactic plane mask applied).

Projected detection rates are presented in Table 4. For fast events (durations between 1 and 10 days), which would include some LGRB reverse shocks and on-axis LGRB afterglows, we use the upper limit on the rate computed by SPT (Guns et al. in prep). For the on-axis LGRB rate we use Lien et al. (2014). For the LGRB and TDE luminosities at 145 GHz we use theoretical predictions (Eftekhari et al. 2022; Metzger et al. 2015) and caution that these are uncertain given the small number of observed events. We take the LLGRB rate from Soderberg et al. (2006), and for the luminosity we use the observed values of GRB 980425/SN 1998bw (Kulkarni et al. 1998) and GRB 171205A/SN 2017iuk (Perley et al. 2017). For AT2018cow-like FBOTs we use observed 100 GHz luminosities (Ho et al. 2022, 2023b) and the volumetric rate from Ho et al. (2023a). For ordinary SNe we use an observationally constrained rate (Li et al. 2011; Perley et al. 2020), and luminosities of the handful of events detected at millimeter wavelengths to date (Berger et al. 2023). We find that ordinary SNe would likely only be detected out to a few Mpc, and thus we do not list these in Table 4, as we expect the detection rate for extragalactic normal SNe to be low. For interacting SNe we use a volumetric rate from the Zwicky Transient Facility (Perley et al. 2020) and a range of luminosities from the modeling in Yurk et al. (2022).

SO will also blindly discover and characterize many stellar flares. Recently, the ACT (Biermann et al. 2024; Li et al. 2023; Naess et al. 2021b) and SPT (Guns et al. 2021; Tandoi et al. 2024) collaborations published blind discoveries of bright transients. We use these to extrapolate the expected stellar flare detection rate for SO with the fully populated LATR, assuming the goal single-observation sensitivity at 93 GHz from Table 3. Assuming that the number density of events is proportional to the source flux density $S^{-3/2}$ and extrapolating from Tandoi et al. (2024), we estimate that SO will detect at least ~ 120 flaring events per year at 5σ at Galactic latitudes $|b| > 5°$. The scale height and flaring rate of stars varies with stellar type (Aganze et al. 2022; Murray et al. 2022), but the intrinsic rate of these events is higher closer to the Galactic plane. However, the expected stellar flare detection rate close

to the Galactic plane is difficult to extrapolate from ACT and SPT results, as both of those surveys had much shallower scan depth near the plane. Estimating the detection rate at $|b| < 5^\circ$ by extrapolating from Li et al. (2023), we estimate that SO will detect at least 50% more events at these low Galactic latitudes. We thus forecast a 5σ stellar flare detection rate for the fully populated SO LATR of at least ~ 180 per year.

With daily updates on source light curves with high time resolution over a wide field, SO will produce a large catalog of flaring stars for investigations of stellar physics. ACT also recently reported an observation of a classical nova (Biermann et al. 2024), one of only a few observations of nova outbursts at millimeter wavelengths (Chomiuk et al. 2014; Diaz et al. 2018; Ivison et al. 1993; Nielbock & Schmidtobreick 2003).

SO will complement a number of concurrent multiwavelength time-domain surveys. During SO operations, high-energy missions including the Space Variables Object Monitor (Cordier et al. 2015) and Einstein Probe (Yuan et al. 2015) will survey the sky in soft X-rays. For transients discovered by SO, these experiments could provide limits on the presence of a high-energy counterpart. In addition, ULTRASAT (Shvartzvald et al. 2024) and UVEX (Kulkarni et al. 2021) will conduct the first wide-field high-cadence surveys in the UV; ULTRASAT will spend a substantial fraction of its observing time in the southern hemisphere. Rubin will provide a wide-field, low-cadence, sensitive multi-band survey. Rubin observations of supernova mass-loss can be combined with SO observations of the terminal explosion. Several wide-field surveys will cover the entire sky to a depth comparable to 2MASS (Moore & Kasliwal 2019), including WINTER (Lourie et al. 2020). Several sensitive wide-field radio transient surveys are planned for the next decade, including the Deep Synoptic Array 2000 (Hallinan et al. 2019), the ASKAP Variables and Slow Transients Survey (Murphy et al. 2013), and the Square Kilometer Array (Fender et al. 2015).

SO adds an important dimension to these complementary experiments with its sensitivity to polarization, which is a useful diagnostic for distinguishing between different classes of sources. The first extragalactic transient found in a blind millimeter survey was linearly polarized with a polarization angle that changed over the duration of the burst (Whitehorn et al. 2016). Such behavior is consistent with emission from a jet, and thus the source may have been a GRB afterglow.

Finally, we note that the wide, blind nature of the SO time-domain survey leaves open the possibility of discovering a wholly new class of transient events.

4 Summary

In this paper, we have described planned infrastructure enhancements relevant to the wide-area survey that will be undertaken with the SO LAT. The fully-populated SO LATR will include four additional MF and two additional UHF optics tubes, as described in Sec. 2. These additions will nearly double the mapping speed over the existing configuration, with the full instrument expected to begin observations in 2028. The final co-added map depth at the conclusion of the survey in 2034 will reach 2.6 $\mu\mathrm{K} \cdot \mathrm{arcmin}$, over roughly 61% of the sky. In addition to the new detectors, the planned infrastructure also includes a new photovoltaic power system, supplying 70% of the power needs of the observatory, as well as an improved data pipeline that will facilitate map delivery to the community and detection of millimeter-wave astrophysical transients. The properties of the fully-populated LATR are summarized in Table 1.

The science goals and forecasts for the wide-area survey conducted with the fully-populated LATR are described in Sec. 3 and summarized in Table 2. The forecasts presented in this work include only statistical errors; our understanding of systematic errors will be refined in future work, particularly as the instrument is now taking data. These include improved constraints on the scale dependence and Gaussianity of the primordial perturbations (reaching $\sigma(f_{\rm NL}^{\rm loc}) = 1$); improved constraints on new light relativistic species (reaching $\sigma(N_{\rm eff}) = 0.045$); tight constraints on the sum of the neutrino masses ($\sigma(\sum m_\nu) = 0.03$ eV, or 0.015 eV in combination with *LiteBIRD*); percent-level constraints on the amplitude of density fluctuations at redshifts $1 < z < 2$ via CMB lensing cross-correlations with LSS surveys; and a tSZ-selected galaxy cluster sample comprising 33,000 objects, including ≈ 200 at $z > 2$. In general, the high-SNR component-separated blackbody temperature and Compton-y maps, as well as the reconstructed gravitational lensing maps, from the complete SO LAT survey will enable a broad range of cosmological and astrophysical science, which we have only briefly covered in this paper. As evidenced by progress in cosmology in recent decades, a data set this rich will enable additional science that has yet to be envisioned or forecast here.

SO will also catalog $\sim 100,000$ AGN and provide high-SNR light curves for $\mathcal{O}(10,000)$ blazars; map the magnetic field structure of hundreds of Galactic molecular clouds; constrain the composition of interstellar dust; detect or strongly constrain the presence of a Planet 9 (with the ability to rule out a 5 $M_\oplus$ Planet 9 out to 500-900 AU); detect or place limits on the population of exo-Oort clouds; and measure the thermal emission from thousands of asteroids, enabling new statistical investigation of asteroid regoliths. Finally, SO will carry out the largest blind survey of transient phenomena in the millimeter to date, which will detect and characterize GRBs, TDEs, FBOTs, and supernovae, as well as on order of a hundred stellar flares per year. The sensitive, large-area maps of millimeter-wavelength emission in both total intensity and linear polarization will enable a wealth of Galactic and extragalactic science, and will open new discovery space in the time domain.

Acknowledgments

This work was supported by the National Science Foundation (Award No. 2153201, UEI GM1XX56LEP58). This work was supported in part by a grant from the Simons Foundation (Award #457687, B.K.). This work was supported in part by a Laboratory Directed Research and Development award from SLAC National Accelerator Laboratory under Department of Energy Contract No. DE-AC02-76SF00515. The research was carried out in part at the Jet Propulsion Laboratory, California Institute of Technology, under a contract with the National Aeronautics and Space Administration (80NM0018D0004). This document was prepared by Simons Observatory using the resources of the Fermi National Accelerator Laboratory (Fermilab), a U.S. Department of Energy, Office of Science, Office of High Energy Physics HEP User Facility. Fermilab is managed by Fermi Forward Discovery Group, LLC, acting under Contract No. 89243024CSC000002. F. Nati acknowledges funding from the European Union (ERC, POLOCALC, 101096035). Views and opinions expressed are however those of the authors only and do not necessarily reflect those of the EU or the ERC. Neither the EU nor the granting authority can be held responsible for them. MH acknowledges financial support from the National Research Foundation of South Africa. JCH acknowledges support from the Sloan Foundation and the Simons Foundation. SEC acknowledges support from the Sloan Foundation. ADH acknowledges support from the Sutton Family Chair in Science,

Christianity and Cultures, from the Faculty of Arts and Science, University of Toronto, and from the Natural Sciences and Engineering Research Council of Canada (NSERC) [RGPIN-2023-05014, DGECR-2023-00180]. This work was supported by a grant from the Simons Foundation (CCA 918271, PBL). AC acknowledges support from the STFC (grant numbers ST/W000997/1 and ST/X006387/1). EH is supported by a Gates Cambridge Scholarship (Grant No. OPP1144 from the Bill & Melinda Gates Foundation). The SISSA group acknowledges partial support by the Italian Space Agency LiteBIRD Project (ASI Grants No. 2020-9-HH.0 and 2016-24-H.1-2018), as well as the InDark and LiteBIRD Initiative of the National Institute for Nuclear Physics, and the RadioForegroundsPlus Project HORIZON-CL4-2023-SPACE-01, GA 101135036. MM acknowledges support from NSF grants AST-2307727 and AST-2153201 and NASA grant 21-ATP21-0145. This work was supported in part by United Kingdom Research and Innovation (UKRI) and the Science and Technology Facilities Council (STFC) (Grant no. ST/X006344/1). CHC acknowledges ANID FONDECYT Postdoc Fellowship 3220255 and BASAL CATA FB210003. NS acknowledges support from DOE award number DE-SC0025309.

We thank Patricia Diego-Palazuelos for facilitating code to run the isotropic cosmic birefringence estimation. Some of the results in this paper have been derived using the `healpy` (Zonca et al. 2019) and `HEALPix` package (Górski et al. 2005), as well as the `PySM` package (The Pan-Experiment Galactic Science Group et al. 2025; Thorne et al. 2017; Zonca et al. 2021).

References

Adame, A. G., et al. 2025, arXiv:2404.03002, JCAP, 2025, 021, DESI 2024 VI: cosmological constraints from the measurements of baryon acoustic oscillations

Ade, P., et al. 2019, arXiv:1808.07445, JCAP, 2019, 056, The Simons Observatory: science goals and forecasts

Ade, P. A. R., et al. 2023, arXiv:2210.05684, Ap. J., 945, 72, BICEP/Keck. XVI. Characterizing Dust Polarization through Correlations with Neutral Hydrogen

—. 2025, arXiv:2407.20982, Ap. J., 978, 130, Analysis of Polarized Dust Emission Using Data from the First Flight of SPIDER

Aganze, C., et al. 2022, arXiv:2204.07621, Ap. J., 934, 73, Beyond the Local Volume. II. Population Scaleheights and Ages of Ultracool Dwarfs in Deep HST/WFC3 Parallel Fields

Aihara, H., et al. 2022, arXiv:2108.13045, PASJ, 74, 247, Third data release of the Hyper Suprime-Cam Subaru Strategic Program

Alexander, J., et al. 2016, arXiv:1608.08632, arXiv e-prints, arXiv:1608.08632, Dark Sectors 2016 Workshop: Community Report

Alexander, K. D., van Velzen, S., Horesh, A., & Zauderer, B. A. 2020, arXiv:2006.01159, SSR, 216, 81, Radio Properties of Tidal Disruption Events

Ali-Haïmoud, Y. & Hirata, C. M. 2011, arXiv:1011.3758, Phys. Rev. D, 83, 043513, HyRec: A fast and highly accurate primordial hydrogen and helium recombination code

Alvarez, M., et al. 2019, BAAS, 51, 482, Unique Probes of Reionization with the CMB: From the First Stars to Fundamental Physics

Alvarez, M. A., Ferraro, S., Hill, J. C., Hložek, R., & Ikape, M. 2021, arXiv:2006.06594, Phys. Rev. D, 103, 063518, Mitigating the optical depth degeneracy using the kinematic Sunyaev-Zel'dovich effect with CMB-S4 data

Andreoni, I., et al. 2022, arXiv:2211.16530, Nature, 612, 430, A very luminous jet from the disruption of a star by a massive black hole

Arkani-Hamed, N., Cohen, T., D'Agnolo, R. T., Hook, A., Kim, H. D., & Pinner, D. 2016, arXiv:1607.06821, Phys. Rev. Lett., 117, 251801, Solving the Hierarchy Problem at Reheating with a Large Number of Degrees of Freedom

Arnaud, M., Pratt, G. W., Piffaretti, R., Böhringer, H., Croston, J. H., & Pointecouteau, E. 2010, arXiv:0910.1234, Ast. and Ap., 517, A92, The universal galaxy cluster pressure profile from a representative sample of nearby systems (REXCESS) and the Y_{SZ} - M_{500} relation

Ashton, P. C., et al. 2018, arXiv:1707.02936, Ap. J., 857, 10, First Observation of the Submillimeter Polarization Spectrum in a Translucent Molecular Cloud

Battaglia, N., Ferraro, S., Schaan, E., & Spergel, D. N. 2017, arXiv:1705.05881, JCAP, 2017, 040, Future constraints on halo thermodynamics from combined Sunyaev-Zel'dovich measurements

Battaglia, N., et al. 2019, arXiv:1903.04647, BAAS, 51, 297, Probing Feedback in Galaxy Formation with Millimeter-wave Observations

Baxter, E. J., Blake, C. H., & Jain, B. 2018, arXiv:1808.00415, A. J., 156, 243, Probing Oort Clouds around Milky Way Stars with CMB Surveys

Bendo, G. J., et al. 2023, arXiv:2301.02584, MNRAS, 522, 2995, The bright extragalactic ALMA redshift survey (BEARS) - II. Millimetre photometry of gravitational lens candidates

Benson, B. A., et al. 2014, arXiv:1407.2973, in Society of Photo-Optical Instrumentation Engineers (SPIE) Conference Series, Vol. 9153, Millimeter, Submillimeter, and Far-Infrared Detectors and Instrumentation for Astronomy VII, ed. W. S. Holland & J. Zmuidzinas, 91531P

Berger, E., et al. 2023, arXiv:2306.09311, Ap. J. Lett., 951, L31, Millimeter Observations of the Type II SN 2023ixf: Constraints on the Proximate Circumstellar Medium

Biermann, E. K., et al. 2024, arXiv:2409.08429, arXiv e-prints, arXiv:2409.08429, The Atacama Cosmology Telescope: Systematic Transient Search of Single Observation Maps

Bleem, L. E., et al. 2022, arXiv:2102.05033, Ap. J. Supp., 258, 36, CMB/kSZ and Compton-y Maps from 2500 $\deg^2$ of SPT-SZ and Planck Survey Data

Bonato, M., et al. 2019, arXiv:1901.08976, MNRAS, 485, 1188, ALMA photometry of extragalactic radio sources

Breuval, L., et al. 2024, arXiv:2404.08038, Ap. J., 973, 30, Small Magellanic Cloud Cepheids Observed with the Hubble Space Telescope Provide a New Anchor for the SH0ES Distance Ladder

Bromberg, O., Nakar, E., & Piran, T. 2011, arXiv:1107.1346, Ap. J. Lett., 739, L55, Are Low-luminosity Gamma-Ray Bursts Generated by Relativistic Jets?

Butterfield, N. O., et al. 2024, arXiv:2306.01681, Ap. J., 963, 130, SOFIA/HAWC+ Far-Infrared Polarimetric Large Area CMZ Exploration Survey. I. General Results from the Pilot Program

Cai, Z.-Y., et al. 2013, arXiv:1303.2335, Ap. J., 768, 21, A Hybrid Model for the Evolution of Galaxies and Active Galactic Nuclei in the Infrared

Cano, Z., Wang, S.-Q., Dai, Z.-G., & Wu, X.-F. 2017, arXiv:1604.03549, Advances in Astronomy, 2017, 8929054, The Observer's Guide to the Gamma-Ray Burst Supernova Connection

Carroll, S. M. 1998, astro-ph/9806099, Phys. Rev. Lett., 81, 3067, Quintessence and the Rest of the World: Suppressing Long-Range Interactions

CCAT-Prime Collaboration, et al. 2023, arXiv:2107.10364, Ap. J. Supp., 264, 7, CCAT-prime Collaboration: Science Goals and Forecasts with Prime-Cam on the Fred Young Submillimeter Telescope

Chandra, P. & Frail, D. A. 2012, arXiv:1110.4124, Ap. J., 746, 156, A Radio-selected Sample of Gamma-Ray Burst Afterglows

Chandran, J., Remazeilles, M., & Barreiro, R. B. 2023, arXiv:2305.10193, MNRAS, 526, 5682, An improved Compton parameter map of thermal Sunyaev-Zeldovich effect from Planck PR4 data

Chevalier, R. A. 1998, Ap. J., 499, 810, Synchrotron Self-Absorption in Radio Supernovae

—. 2012, arXiv:1204.3300, Ap. J. Lett., 752, L2, Common Envelope Evolution Leading to Supernovae with Dense Interaction

Chiang, C.-T. & Slosar, A. 2018, arXiv:1811.03624, arXiv e-prints, arXiv:1811.03624, Inferences of H_0 in presence of a non-standard recombination

Chichura, P. M., et al. 2022, arXiv:2202.01406, Ap. J., 936, 173, Asteroid Measurements at Millimeter Wavelengths with the South Pole Telescope

Chluba, J., Nagai, D., Sazonov, S., & Nelson, K. 2012, arXiv:1205.5778, MNRAS, 426, 510, A fast and accurate method for computing the Sunyaev-Zel'dovich signal of hot galaxy clusters

Chluba, J. & Thomas, R. M. 2011, arXiv:1010.3631, MNRAS, 412, 748, Towards a complete treatment of the cosmological recombination problem

Choi, S. K., et al. 2020, arXiv:2007.07289, JCAP, 2020, 045, The Atacama Cosmology Telescope: a measurement of the Cosmic Microwave Background power spectra at 98 and 150 GHz

Chomiuk, L., et al. 2014, arXiv:1410.3473, Nature, 514, 339, Binary orbits as the driver of γ-ray emission and mass ejection in classical novae

—. 2021, arXiv:2107.06251, Ap. J. Supp., 257, 49, Classical Novae at Radio Wavelengths

Clancy, J., et al. 2023, arXiv:2303.02788, MNRAS, 524, 3712, Polarization fraction of Planck Galactic cold clumps and forecasts for the Simons Observatory

Clark, S., Heiles, C., & Robishaw, T. 2019, BAAS, 51, 390, Magnetic Fields and Polarization in the Diffuse Interstellar Medium

Clark, S. E. & Hensley, B. S. 2019, arXiv:1909.11673, Ap. J., 887, 136, Mapping the Magnetic Interstellar Medium in Three Dimensions over the Full Sky with Neutral Hydrogen

Clark, S. E., Hill, J. C., Peek, J. E. G., Putman, M. E., & Babler, B. L. 2015, arXiv:1508.07005, Phys. Rev. Lett., 115, 241302, Neutral Hydrogen Structures Trace Dust Polarization Angle: Implications for Cosmic Microwave Background Foregrounds

Clark, S. E., Kim, C.-G., Hill, J. C., & Hensley, B. S. 2021, arXiv:2105.00120, Ap. J., 919, 53, The Origin of Parity Violation in Polarized Dust Emission and Implications for Cosmic Birefringence

Cobb, B. E., Bailyn, C. D., van Dokkum, P. G., & Natarajan, P. 2006, astro-ph/0603832, Ap. J. Lett., 645, L113, SN 2006aj and the Nature of Low-Luminosity Gamma-Ray Bursts

Cordier, B., et al. 2015, arXiv:1512.03323, arXiv e-prints, arXiv:1512.03323, The SVOM gamma-ray burst mission

Córdova Rosado, R., et al. 2024, arXiv:2307.06352, Ap. J., 960, 96, The Atacama Cosmology Telescope: Galactic Dust Structure and the Cosmic PAH Background in Cross-correlation with WISE

Cortes, P. C., et al. 2024, ALMA Technical Handbook, Tech. Rep. ALMA Doc. 11.3, ver. 1.4

Coulton, W., et al. 2024a, arXiv:2307.01258, Phys. Rev. D, 109, 063530, Atacama Cosmology Telescope: High-resolution component-separated maps across one third of the sky

Coulton, W. R., et al. 2024b, arXiv:2410.19046, arXiv e-prints, arXiv:2410.19046, The Atacama Cosmology Telescope: A measurement of galaxy cluster temperatures through relativistic corrections to the thermal Sunyaev-Zeldovich effect

Crutcher, R. M. 2012, ARRA, 50, 29, Magnetic Fields in Molecular Clouds

Cukierman, A. J., Clark, S. E., & Halal, G. 2023, arXiv:2208.07382, Ap. J., 946, 106, Magnetic Misalignment of Interstellar Dust Filaments

Dark Energy Survey Collaboration, et al. 2016, arXiv:1601.00329, MNRAS, 460, 1270, The Dark Energy Survey: more than dark energy - an overview

Dartois, E., et al. 2024, Nature Astronomy, 8, 359, Spectroscopic sizing of interstellar icy grains with JWST

De Zotti, G., et al. 2019a, arXiv:1904.04531, BAAS, 51, 50, Early evolution of galaxies and of large-scale structure from CMB experiments

—. 2019b, arXiv:1904.05769, BAAS, 51, 54, Radio sources in next-generation CMB surveys

Dermer, C. D. & Atoyan, A. 2001, astro-ph/0107200, arXiv e-prints, astro, High-Energy Neutrino Production through Photopion Processes in Blazars

Dermer, C. D., Chiang, J., & Böttcher, M. 1999, astro-ph/9804174, Ap. J., 513, 656, Fireball Loading and the Blast-Wave Model of Gamma-Ray Bursts

Dermer, C. D. & Schlickeiser, R. 1993, Ap. J., 416, 458, Model for the High-Energy Emission from Blazars

Di Valentino, E., et al. 2021a, arXiv:2008.11284, Astroparticle Physics, 131, 102605, Cosmology Intertwined II: The hubble constant tension

—. 2021b, arXiv:2103.01183, Classical and Quantum Gravity, 38, 153001, In the realm of the Hubble tension-a review of solutions

Diaz, M. P., Abraham, Z., Ribeiro, V. A. R. M., Beaklini, P. P. B., & Takeda, L. 2018, arXiv:1808.01848, MNRAS, 480, L54, The structure of a recent nova shell as observed by ALMA

Dickinson, C., et al. 2018, arXiv:1802.08073, New Ast. Rev., 80, 1, The State-of-Play of Anomalous Microwave Emission (AME) research

Diego-Palazuelos, P., et al. 2022, arXiv:2201.07682, Phys. Rev. Lett., 128, 091302, Cosmic Birefringence from the Planck Data Release 4

—. 2023, arXiv:2210.07655, JCAP, 2023, 044, Robustness of cosmic birefringence measurement against Galactic foreground emission and instrumental systematics

Doré, O., et al. 2014, arXiv:1412.4872, arXiv e-prints, arXiv:1412.4872, Cosmology with the SPHEREX All-Sky Spectral Survey

Draine, B. T. & Hensley, B. 2013, arXiv:1205.7021, Ap. J., 765, 159, Magnetic Nanoparticles in the Interstellar Medium: Emission Spectrum and Polarization

Draine, B. T. & Hensley, B. S. 2016, arXiv:1605.06671, Ap. J., 831, 59, Quantum Suppression of Alignment in Ultrasmall Grains: Microwave Emission from Spinning Dust will be Negligibly Polarized

—. 2021a, arXiv:2009.11314, Ap. J., 909, 94, The Dielectric Function of "Astrodust" and Predictions for Polarization in the 3.4 and 10 μm Features

—. 2021b, arXiv:2101.07277, Ap. J., 919, 65, Using the Starlight Polarization Efficiency Integral to Constrain Shapes and Porosities of Interstellar Grains

Dvorkin, C., et al. 2019, arXiv:1903.03689, BAAS, 51, 64, Neutrino Mass from Cosmology: Probing Physics Beyond the Standard Model

Eftekhari, T., et al. 2022, arXiv:2110.05494, Ap. J., 935, 16, Extragalactic Millimeter Transients in the Era of Next-generation CMB Surveys

Erler, J., Basu, K., Chluba, J., & Bertoldi, F. 2018, arXiv:1709.01187, MNRAS, 476, 3360, Planck's view on the spectrum of the Sunyaev-Zeldovich effect

Eskilt, J. R. & Komatsu, E. 2022, arXiv:2205.13962, Phys. Rev. D, 106, 063503, Improved constraints on cosmic birefringence from the WMAP and Planck cosmic microwave background polarization data

Essig, R., et al. 2013, arXiv:1311.0029, arXiv e-prints, arXiv:1311.0029, Dark Sectors and New, Light, Weakly-Coupled Particles

Euclid Collaboration, et al. 2024, arXiv:2405.13491, arXiv e-prints, arXiv:2405.13491, Euclid. I. Overview of the Euclid mission

Everett, W. B., et al. 2020, arXiv:2003.03431, Ap. J., 900, 55, Millimeter-wave Point Sources from the 2500 Square Degree SPT-SZ Survey: Catalog and Population Statistics

Fang, X., Eifler, T., Schaan, E., Huang, H.-J., Krause, E., & Ferraro, S. 2022, arXiv:2108.00658, MNRAS, 509, 5721, Cosmology from clustering, cosmic shear, CMB lensing, and cross correlations: combining Rubin observatory and Simons Observatory

Fender, R., Stewart, A., Macquart, J. P., Donnarumma, I., Murphy, T., Deller, A., Paragi, Z., & Chatterjee, S. 2015, arXiv:1507.00729, in Advancing Astrophysics with the Square Kilometre Array (AASKA14), 51

Fernandes, R. B., Mulders, G. D., Pascucci, I., Mordasini, C., & Emsenhuber, A. 2019, arXiv:1812.05569, Ap. J., 874, 81, Hints for a Turnover at the Snow Line in the Giant Planet Occurrence Rate

Ferraro, S. & Smith, K. M. 2018, arXiv:1803.07036, PRD, 98, 123519, Characterizing the epoch of reionization with the small-scale CMB: Constraints on the optical depth and duration

Ferreira, E. G. M. 2021, arXiv:2005.03254, AAPR, 29, 7, Ultra-light dark matter

Fienga, A., Di Ruscio, A., Bernus, L., Deram, P., Durante, D., Laskar, J., & Iess, L. 2020, Ast. and Ap., 640, A6, New constraints on the location of P9 obtained with the INPOP19a planetary ephemeris

Fissel, L., et al. 2019, arXiv:1903.08757, Astro2020: Decadal Survey on Astronomy and Astrophysics, 2020, 193, Studying Magnetic Fields in Star Formation and the Turbulent Interstellar Medium

Freedman, W. L., Madore, B. F., Jang, I. S., Hoyt, T. J., Lee, A. J., & Owens, K. A. 2024, arXiv:2408.06153, arXiv e-prints, arXiv:2408.06153, Status Report on the Chicago-Carnegie Hubble Program (CCHP): Three Independent Astrophysical Determinations of the Hubble Constant Using the James Webb Space Telescope

Galitzki, N., et al. 2024, arXiv:2405.05550, Ap. J. Supp., 274, 33, The Simons Observatory: Design, Integration, and Testing of the Small Aperture Telescopes

Galli, S., Pogosian, L., Jedamzik, K., & Balkenhol, L. 2022, arXiv:2109.03816, Phys. Rev. D, 105, 023513, Consistency of Planck, ACT, and SPT constraints on magnetically assisted recombination and forecasts for future experiments

Glenn, J., et al. 2010, arXiv:1009.5675, MNRAS, 409, 109, HerMES: deep galaxy number counts from a P(D) fluctuation analysis of SPIRE Science Demonstration Phase observations

Gluscevic, V., et al. 2019, arXiv:1903.05140, BAAS, 51, 134, Cosmological Probes of Dark Matter Interactions: The Next Decade

Goldreich, P. & Kylafis, N. D. 1981, Ap. J. Lett., 243, L75, On mapping the magnetic field direction in molecular clouds by polarization measurements

Górski, K. M., Hivon, E., Banday, A. J., Wandelt, B. D., Hansen, F. K., Reinecke, M., & Bartelmann, M. 2005, arXiv:astro-ph/0409513, Ap. J., 622, 759, HEALPix: A Framework for High-Resolution Discretization and Fast Analysis of Data Distributed on the Sphere

Gralla, M. B., et al. 2020, arXiv:1905.04592, Ap. J., 893, 104, Atacama Cosmology Telescope: Dusty Star-forming Galaxies and Active Galactic Nuclei in the Equatorial Survey

Green, D., et al. 2019, arXiv:1903.04763, BAAS, 51, 159, Messengers from the Early Universe: Cosmic Neutrinos and Other Light Relics

Grin, D., Amin, M. A., Gluscevic, V., Hlozek, R., Marsh, D. J. E., Poulin, V., Prescod-Weinstein, C., & Smith, T. 2019, arXiv:1904.09003, BAAS, 51, 567, Gravitational probes of ultra-light axions

Grohs, E., Bond, J. R., Cooke, R. J., Fuller, G. M., Meyers, J., & Paris, M. W. 2019, arXiv:1903.09187, in BAAS, Vol. 51, 412

Guan, Y., et al. 2021, arXiv:2105.05267, Ap. J., 920, 6, The Atacama Cosmology Telescope: Microwave Intensity and Polarization Maps of the Galactic Center

—. 2024, arXiv:2406.10905, arXiv e-prints, arXiv:2406.10905, Simons Observatory: Observatory Scheduler and Automated Data Processing

Gudmundsson, J. E., et al. 2021, arXiv:2009.10138, Appl. Optics, 60, 823, The Simons Observatory: modeling optical systematics in the Large Aperture Telescope

Guillet, V., et al. 2018, arXiv:1710.04598, Ast. and Ap., 610, A16, Dust models compatible with Planck intensity and polarization data in translucent lines of sight

Guns, S., et al. 2021, arXiv:2103.06166, Ap. J., 916, 98, Detection of Galactic and Extragalactic Millimeter-wavelength Transient Sources with SPT-3G

Hadzhiyska, B., et al. 2024, arXiv:2407.07152, arXiv e-prints, arXiv:2407.07152, Evidence for large baryonic feedback at low and intermediate redshifts from kinematic Sunyaev-Zel'dovich observations with ACT and DESI photometric galaxies

Halal, G., Clark, S. E., Cukierman, A., Beck, D., & Kuo, C.-L. 2024, arXiv:2306.10107, Ap. J., 961, 29, Filamentary Dust Polarization and the Morphology of Neutral Hydrogen Structures

Hallinan, G., et al. 2019, arXiv:1907.07648, in Bulletin of the American Astronomical Society, Vol. 51, 255

Hanany, S., et al. 2019, arXiv:1902.10541, arXiv e-prints, arXiv:1902.10541, PICO: Probe of Inflation and Cosmic Origins

Haridas, S. K., et al. 2024, arXiv:2407.09669, arXiv e-prints, arXiv:2407.09669, The Simons Observatory: Dark Characterization of the Large Aperture Telescope

Harrington, K., et al. 2016, arXiv:1608.08234, in Society of Photo-Optical Instrumentation Engineers (SPIE) Conference Series, Vol. 9914, Millimeter, Submillimeter, and Far-Infrared Detectors and Instrumentation for Astronomy VIII, ed. W. S. Holland & J. Zmuidzinas, 99141K

Hensley, B., et al. 2019, BAAS, 51, 224, Determining the Composition of Interstellar Dust with Far-Infrared Polarimetry

Hensley, B. S. & Draine, B. T. 2023, arXiv:2208.12365, Ap. J., 948, 55, The Astrodust+PAH Model: A Unified Description of the Extinction, Emission, and Polarization from Dust in the Diffuse Interstellar Medium

Hensley, B. S., et al. 2022, arXiv:2111.02425, Ap. J., 929, 166, The Simons Observatory: Galactic Science Goals and Forecasts

HEPAP Subcommittee Collaboration. 2014, Building for Discovery: Strategic Plan for U.S. Particle Physics in the Global Context, https://www.usparticlephysics.org/wp-content/uploads/2018/03/FINAL_P5_Report_053014.pdf

—. 2023, Exploring the Quantum Universe: Pathways to Innovation and Discovery in Particle Physics, https://www.usparticlephysics.org/2023-p5-report/assets/pdf/2023_P5_Report_Single_Pages.pdf

HERA Collaboration, et al. 2023, arXiv:2210.04912, Ap. J., 945, 124, Improved Constraints on the 21 cm EoR Power Spectrum and the X-Ray Heating of the IGM with HERA Phase I Observations

Herranz, D., Sanz, J. L., Hobson, M. P., Barreiro, R. B., Diego, J. M., Martínez-González, E., & Lasenby, A. N. 2002, astro-ph/0203486, MNRAS, 336, 1057, Filtering techniques for the detection of Sunyaev-Zel'dovich clusters ¡br/¿ in multifrequency maps

Hertig, E., et al. 2024, arXiv:2405.01621, Phys. Rev. D, 110, 043532, The Simons Observatory: Combining cross-spectral foreground cleaning with multitracer B-mode delensing for improved constraints on inflation

Hervías-Caimapo, C., Cukierman, A. J., Diego-Palazuelos, P., Huffenberger, K. M., & Clark, S. E. 2025, arXiv:2408.06214, Phys. Rev. D, 111, 083532, Modeling parity-violating spectra in Galactic dust polarization with filaments and its applications to cosmic birefringence searches

Hervías-Caimapo, C., et al. 2024, arXiv:2301.07651, MNRAS, 529, 3020, The Atacama cosmology telescope: flux upper limits from a targeted search for extragalactic transients

Heywood, I., et al. 2019, arXiv:1909.05534, Nature, 573, 235, Inflation of 430-parsec bipolar radio bubbles in the Galactic Centre by an energetic event

Hill, C. A., Bruno, S. M. M., Simon, S. M., et al. 2018, arXiv:1806.04316, in SPIE Conference Series, Vol. 10708, 1070842

Hill, J. C., et al. 2022, arXiv:2109.04451, Phys. Rev. D, 105, 123536, Atacama Cosmology Telescope: Constraints on prerecombination early dark energy

Hilton, M., et al. 2021, arXiv:2009.11043, Ap. J. Supp., 253, 3, The Atacama Cosmology Telescope: A Catalog of ¿4000 Sunyaev–Zel'dovich Galaxy Clusters

Ho, A. Y. Q., et al. 2019, arXiv:1810.10880, Ap. J., 871, 73, AT2018cow: A Luminous Millimeter Transient

—. 2022, arXiv:2110.05490, Ap. J., 932, 116, Luminous Millimeter, Radio, and X-Ray Emission from ZTF 20acigmel (AT 2020xnd)

—. 2023a, arXiv:2105.08811, Ap. J., 949, 120, A Search for Extragalactic Fast Blue Optical Transients in ZTF and the Rate of AT2018cow-like Transients

—. 2023b, arXiv:2311.10195, Nature, 623, 927, Minutes-duration optical flares with supernova luminosities

Hoang, T., Lazarian, A., & Martin, P. G. 2013, arXiv:1305.0276, Ap. J., 779, 152, Constraint on the Polarization of Electric Dipole Emission from Spinning Dust

Holder, G., Berger, E., Bleem, L., Crawford, T. M., Scott, D., & Whitehorn, N. 2019, BAAS, 51, 331, Tracking the time-variable Millimeter-wave sky with CMB experiments

Hood, J. C., I., et al. 2023, arXiv:2302.14749, Ap. J. Lett., 945, L23, Simultaneous Millimeter-wave, Gamma-Ray, and Optical Monitoring of the Blazar PKS 2326-502 during a Flaring State

Huffenberger, K. M., Rotti, A., & Collins, D. C. 2020, arXiv:1906.10052, Ap. J., 899, 31, The Power Spectra of Polarized, Dusty Filaments

IceCube Collaboration, et al. 2018, arXiv:1807.08794, Science, 361, 147, Neutrino emission from the direction of the blazar TXS 0506+056 prior to the IceCube-170922A alert

Idicherian Lonappan, A. 2025, arXiv:2503.04708, Improving Cosmic Birefringence Constraints via Delensing

Ivison, R. J., Hughes, D. H., Lloyd, H. M., Bang, M. K., & Bode, M. F. 1993, MNRAS, 263, L43, Millimetre and submillimetre continuum observations of Nova Cygni 1992 : a new test of mass ejection models.

Johnston, K. J., Seidelmann, P. K., & Wade, C. M. 1982, A. J., 87, 1593, Observations of 1 Ceres and 2 Pallas at centimeter wavelengths

Keihm, S., Kamp, L., Gulkis, S., Hofstadter, M., Lee, S., Janssen, M., & Choukroun, M. 2013, Icarus, 226, 1086, Reconciling main belt asteroid spectral flux density measurements with a self-consistent thermophysical model

Kiehlmann, S., et al. 2024, arXiv:2407.09647, arXiv e-prints, arXiv:2407.09647, PKS 2131-021 – Discovery of Strong Coherent Sinusoidal Variations from Radio to Optical Frequencies: Compelling Evidence for a Blazar Supermassive Black Hole Binary

Kitayama, T., et al. 2023, arXiv:2209.09503, PASJ, 75, 311, Galaxy clusters at z $\sim$ 1 imaged by ALMA with the Sunyaev-Zel'dovich effect

Knox, L. & Millea, M. 2020, arXiv:1908.03663, Phys. Rev. D, 101, 043533, Hubble constant hunter's guide

Kou, R. & Lewis, A. 2025, arXiv:2410.16185, JCAP, 2025, 033, A flexible parameterization to test early physics solutions to the Hubble tension with future CMB data

Kulkarni, S. R., et al. 1998, Nature, 395, 663, Radio emission from the unusual supernova 1998bw and its association with the γ-ray burst of 25 April 1998

—. 2021, arXiv:2111.15608, arXiv e-prints, arXiv:2111.15608, Science with the Ultraviolet Explorer (UVEX)

Lagache, G., Béthermin, M., Montier, L., Serra, P., & Tucci, M. 2020, arXiv:1911.09466, Ast. and Ap., 642, A232, Impact of polarised extragalactic sources on the measurement of CMB B-mode anisotropies

Laskar, T., et al. 2018, arXiv:1808.09476, Ap. J., 862, 94, First ALMA Light Curve Constrains Refreshed Reverse Shocks and Jet Magnetization in GRB 161219B

—. 2019, arXiv:1904.07261, Ap. J. Lett., 878, L26, ALMA Detection of a Linearly Polarized Reverse Shock in GRB 190114C

Lazarian, A. & Draine, B. T. 2000, astro-ph/0003312, Ap. J. Lett., 536, L15, Resonance Paramagnetic Relaxation and Alignment of Small Grains

Lebofsky, L. A., et al. 1986, Icarus, 68, 239, A refined "standard" thermal model for asteroids based on observations of 1 Ceres and 2 Pallas

Lee, A., et al. 2019, in , Vol. 51, 286

Lee, E. & Chluba, J. 2024, arXiv:2403.18530, JCAP, 2024, 040, The SZ effect with anisotropic distributions and high energy electrons

Lei, M. & Clark, S. E. 2024, arXiv:2312.03846, Ap. J., 972, 66, A New Constraint on the Relative Disorder of Magnetic Fields between Neutral Interstellar Medium Phases

Li, W., Chornock, R., Leaman, J., Filippenko, A. V., Poznanski, D., Wang, X., Ganeshalingam, M., & Mannucci, F. 2011, arXiv:1006.4613, MNRAS, 412, 1473, Nearby supernova rates from the Lick Observatory Supernova Search - III. The rate-size relation, and the rates as a function of galaxy Hubble type and colour

Li, Y., et al. 2023, arXiv:2303.04767, Ap. J., 956, 36, The Atacama Cosmology Telescope: Systematic Transient Search of 3 Day Maps

Liang, E., Zhang, B., Virgili, F., & Dai, Z. G. 2007, astro-ph/0605200, Ap. J., 662, 1111, Low-Luminosity Gamma-Ray Bursts as a Unique Population: Luminosity Function, Local Rate, and Beaming Factor

Lien, A., Sakamoto, T., Gehrels, N., Palmer, D. M., Barthelmy, S. D., Graziani, C., & Cannizzo, J. K. 2014, arXiv:1311.4567, Ap. J., 783, 24, Probing the Cosmic Gamma-Ray Burst Rate with Trigger Simulations of the Swift Burst Alert Telescope

Liodakis, I., Romani, R. W., Filippenko, A. V., Kiehlmann, S., Max-Moerbeck, W., Readhead, A. C. S., & Zheng, W. 2018, arXiv:1808.05625, MNRAS, 480, 5517, Multiwavelength cross-correlations and flaring activity in bright blazars

Lister, M. L., Aller, M. F., Aller, H. D., Hodge, M. A., Homan, D. C., Kovalev, Y. Y., Pushkarev, A. B., & Savolainen, T. 2018, arXiv:1711.07802, Ap. J. Supp., 234, 12, MOJAVE. XV. VLBA 15 GHz Total Intensity and Polarization Maps of 437 Parsec-scale AGN Jets from 1996 to 2017

LiteBIRD Collaboration, et al. 2023, arXiv:2202.02773, Progress of Theoretical and Experimental Physics, 2023, 042F01, Probing cosmic inflation with the LiteBIRD cosmic microwave background polarization survey

Lourie, N. P., et al. 2020, arXiv:2102.01109, in Society of Photo-Optical Instrumentation Engineers (SPIE) Conference Series, Vol. 11447, Society of Photo-Optical Instrumentation Engineers (SPIE) Conference Series, 114479K

LSST Science Collaboration, et al. 2009, arXiv:0912.0201, ArXiv e-prints, LSST Science Book, Version 2.0

Lue, A., Wang, L., & Kamionkowski, M. 1999, astro-ph/9812088, Phys. Rev. Lett., 83, 1506, Cosmological Signature of New Parity-Violating Interactions

Luhman, K. L. 2014, Ap. J., 781, 4, A Search for a Distant Companion to the Sun with the Wide-field Infrared Survey Explorer

Lynch, G. P., Knox, L., & Chluba, J. 2024, arXiv:2404.05715, Phys. Rev. D, 110, 063518, Reconstructing the recombination history by combining early and late cosmological probes

MacCrann, N., et al. 2024, arXiv:2405.01188, MNRAS, 532, 4247, The Atacama Cosmology Telescope: Reionization kSZ trispectrum methodology and limits

MacGregor, M. A., et al. 2017, arXiv:1705.05867, Ap. J., 842, 8, A Complete ALMA Map of the Fomalhaut Debris Disk

Madhavacheril, M. S., Battaglia, N., & Miyatake, H. 2017, arXiv:1708.07502, Phys. Rev. D, 96, 103525, Fundamental physics from future weak-lensing calibrated Sunyaev-Zel'dovich galaxy cluster counts

Maeda, K., Michiyama, T., Chandra, P., Ryder, S., Kuncarayakti, H., Hiramatsu, D., & Imanishi, M. 2023, arXiv:2301.07357, Ap. J. Lett., 945, L3, Resurrection of Type IIL Supernova 2018ivc: Implications for a Binary Evolution Sequence Connecting Hydrogen-rich and Hydrogen-poor Progenitors

Maeda, K., et al. 2021, arXiv:2106.11618, Ap. J., 918, 34, The Final Months of Massive Star Evolution from the Circumstellar Environment around SN Ic 2020oi

Mantz, A. et al. 2019, arXiv:1903.05606, in BAAS, Vol. 51, 279

Maraschi, L., Ghisellini, G., & Celotti, A. 1992, Ap. J. Lett., 397, L5, A Jet Model for the Gamma-Ray–emitting Blazar 3C 279

Margalit, B. & Quataert, E. 2021, arXiv:2111.00012, Ap. J. Lett., 923, L14, Thermal Electrons in Mildly Relativistic Synchrotron Blast Waves

—. 2024, arXiv:2403.07048, Ap. J., 977, 134, The Peak Frequency and Luminosity of Synchrotron Emitting Shocks: From Nonrelativistic to Ultrarelativistic Explosions

Margutti, R., et al. 2019, arXiv:1810.10720, Ap. J., 872, 18, An Embedded X-Ray Source Shines through the Aspherical AT 2018cow: Revealing the Inner Workings of the Most Luminous Fast-evolving Optical Transients

Marsh, D. J. E. 2016, arXiv:1510.07633, Phys. Rep., 643, 1, Axion cosmology

McCarthy, F. & Hill, J. C. 2024, arXiv:2307.01043, Phys. Rev. D, 109, 023528, Component-separated, CIB-cleaned thermal Sunyaev-Zel'dovich maps from Planck PR4 data with a flexible public needlet ILC pipeline

Meerburg, P. D., et al. 2019, arXiv:1903.04409, BAAS, 51, 107, Primordial Non-Gaussianity

Melin, J. B., Bartlett, J. G., & Delabrouille, J. 2006, astro-ph/0602424, Ast. and Ap., 459, 341, Catalog extraction in SZ cluster surveys: a matched filter approach

Mellema, G., et al. 2013, arXiv:1210.0197, Experimental Astronomy, 36, 235, Reionization and the Cosmic Dawn with the Square Kilometre Array

Merloni, A., et al. 2024, arXiv:2401.17274, Ast. and Ap., 682, A34, The SRG/eROSITA all-sky survey. First X-ray catalogues and data release of the western Galactic hemisphere

Metzger, B. D., Williams, P. K. G., & Berger, E. 2015, arXiv:1502.01350, Ap. J., 806, 224, Extragalactic Synchrotron Transients in the Era of Wide-field Radio Surveys. I. Detection Rates and Light Curve Characteristics

Michel, P., DeMeo, F. E., & Bottke, W. F. 2015, in Asteroids IV (University of Arizona Press), 3–10

Minami, Y. & Komatsu, E. 2020, arXiv:2011.11254, Phys. Rev. Lett., 125, 221301, New Extraction of the Cosmic Birefringence from the Planck 2018 Polarization Data

Montefalcone, G., Wallisch, B., & Freese, K. 2025, arXiv:2501.13788, Free-Streaming Neutrinos and Their Phase Shift in Current and Future CMB Power Spectra

Moore, A. M. & Kasliwal, M. M. 2019, Nature Astronomy, 3, 109, Unveiling the dynamic infrared sky

Mroczkowski, T., et al. 2019, arXiv:1811.02310, SSR, 215, 17, Astrophysics with the Spatially and Spectrally Resolved Sunyaev-Zeldovich Effects. A Millimetre/Submillimetre Probe of the Warm and Hot Universe

Mücke, A. & Protheroe, R. J. 2001, astro-ph/0004052, Astroparticle Physics, 15, 121, A proton synchrotron blazar model for flaring in Markarian 501

Münchmeyer, M., Madhavacheril, M. S., Ferraro, S., Johnson, M. C., & Smith, K. M. 2019, arXiv:1810.13424, Phys. Rev. D, 100, 083508, Constraining local non-Gaussianities with kinetic Sunyaev-Zel'dovich tomography

Murase, K., Ioka, K., Nagataki, S., & Nakamura, T. 2008, arXiv:0801.2861, Phys. Rev. D, 78, 023005, High-energy cosmic-ray nuclei from high- and low-luminosity gamma-ray bursts and implications for multimessenger astronomy

Murphy, T., et al. 2013, arXiv:1207.1528, PASA, 30, e006, VAST: An ASKAP Survey for Variables and Slow Transients

Murray, C. A., et al. 2022, arXiv:2204.10417, MNRAS, 513, 2615, A study of flares in the ultra-cool regime from SPECULOOS-South

Muñoz, J. B., Dvorkin, C., DePorzio, N., Green, D., Meyers, J., & Xu, W. L. 2021, Snowmass 2021 Letter of Interest: Light but Massive Relics in Cosmology

Naess, S., et al. 2021a, arXiv:2104.10264, Ap. J., 923, 224, The Atacama Cosmology Telescope: A Search for Planet 9

—. 2021b, arXiv:2012.14347, Ap. J., 915, 14, The Atacama Cosmology Telescope: Detection of Millimeter-wave Transient Sources

Nakar, E. 2015, arXiv:1503.00441, Ap. J., 807, 172, A Unified Picture for Low-luminosity and Long Gamma-Ray Bursts Based on the Extended Progenitor of llGRB 060218/SN 2006aj

Nakar, E. & Piran, T. 2004, astro-ph/0403461, MNRAS, 353, 647, Early afterglow emission from a reverse shock as a diagnostic tool for gamma-ray burst outflows

Namikawa, T., et al. 2022, arXiv:2110.09730, Phys. Rev. D, 105, 023511, Simons Observatory: Constraining inflationary gravitational waves with multitracer B -mode delensing

Naokawa, F. & Namikawa, T. 2023, arXiv:2305.13976, Phys. Rev. D, 108, 063525, Gravitational lensing effect on cosmic birefringence

Nederlander, A., et al. 2021, arXiv:2101.08849, Ap. J., 917, 5, Resolving Structure in the Debris Disk around HD 206893 with ALMA

Nibauer, J., Baxter, E., & Jain, B. 2020, arXiv:1912.10498, A. J., 159, 210, The Statistics of Extended Debris Disks Measured with Gaia and Planck

Nibauer, J., Baxter, E. J., Jain, B., Van Saders, J. L., Beaton, R. L., & Teske, J. K. 2021, arXiv:2010.07241, Ap. J., 907, 116, Statistics of the Chemical Composition of Solar Analog Stars and Links to Planet Formation

Nielbock, M. & Schmidtobreick, L. 2003, astro-ph/0302244, Ast. and Ap., 400, L5, Looking for dust and molecules in Nova V4743 Sagittarii

Oort, J. H. 1950, Bull. Astro. Inst. Netherlands, 11, 91, The structure of the cloud of comets surrounding the Solar System and a hypothesis concerning its origin

Orlowski-Scherer, J., et al. 2024, arXiv:2306.05468, Ap. J., 964, 138, The Atacama Cosmology Telescope: Millimeter Observations of a Population of Asteroids or: ACTeroids

Paine, S. 2019, The am atmospheric model

Parshley, S. C. et al. 2018, arXiv:1807.06678, in SPIE Conference Series, Vol. 10700, 1070041

Particle Data Group Collaboration. 2014, Chin. Phys., C38, 090001, Review of Particle Physics

Pelgrims, V., Clark, S. E., Hensley, B. S., Panopoulou, G. V., Pavlidou, V., Tassis, K., Eriksen, H. K., & Wehus, I. K. 2021, arXiv:2101.09291, Ast. and Ap., 647, A16, Evidence for line-of-sight frequency decorrelation of polarized dust emission in Planck data

Perley, D. A., Schulze, S., & de Ugarte Postigo, A. 2017, GRB Coordinates Network, 22252, 1, GRB 171205A: ALMA observations.

Perley, D. A., et al. 2014, arXiv:1307.4401, Ap. J., 781, 37, The Afterglow of GRB 130427A from 1 to 10^{16} GHz

—. 2020, arXiv:2009.01242, Ap. J., 904, 35, The Zwicky Transient Facility Bright Transient Survey. II. A Public Statistical Sample for Exploring Supernova Demographics

—. 2021, arXiv:2103.01968, MNRAS, 508, 5138, Real-time discovery of AT2020xnd: a fast, luminous ultraviolet transient with minimal radioactive ejecta

Piran, T. 2004, astro-ph/0405503, Reviews of Modern Physics, 76, 1143, The physics of gamma-ray bursts

Planck Collaboration. 2016, arXiv:1502.01598, Astron. Astrophys., 594, A27, Planck 2015 results. XXVII. The Second Planck Catalogue of Sunyaev-Zeldovich Sources

Planck Collaboration, et al. 2014, arXiv:1303.5073, Ast. and Ap., 571, A13, Planck 2013 results. XIII. Galactic CO emission

—. 2016a, arXiv:1502.01589, Ast. and Ap., 594, A13, Planck 2015 results. XIII. Cosmological parameters

—. 2016b, arXiv:1502.01596, Ast. and Ap., 594, A22, Planck 2015 results. XXII. A map of the thermal Sunyaev-Zeldovich effect

—. 2016c, arXiv:1507.02058, Ast. and Ap., 594, A26, Planck 2015 results. XXVI. The Second Planck Catalogue of Compact Sources

—. 2020a, arXiv:1807.06205, Ast. and Ap., 641, A1, Planck 2018 results. I. Overview and the cosmological legacy of Planck

—. 2020b, arXiv:1807.06209, Ast. and Ap., 641, A6, Planck 2018 results. VI. Cosmological parameters

—. 2020c, arXiv:1801.04945, Ast. and Ap., 641, A11, Planck 2018 results. XI. Polarized dust foregrounds

—. 2020d, arXiv:1807.06212, Ast. and Ap., 641, A12, Planck 2018 results. XII. Galactic astrophysics using polarized dust emission

Prabhu, K., et al. 2024, arXiv:2403.17925, Ap. J., 973, 4, Testing the ΛCDM Cosmological Model with Forthcoming Measurements of the Cosmic Microwave Background with SPT-3G

Prentice, S. J., et al. 2018, arXiv:1807.05965, Ap. J. Lett., 865, L3, The Cow: Discovery of a Luminous, Hot, and Rapidly Evolving Transient

Qu, F. J., Sherwin, B. D., Darwish, O., Namikawa, T., & Madhavacheril, M. S. 2023, arXiv:2208.04253, Phys. Rev. D, 107, 123540, Probing early structure and model-independent neutrino mass with high-redshift CMB lensing mass maps

Quataert, E. & Shiode, J. 2012, arXiv:1202.5036, MNRAS, 423, L92, Wave-driven mass loss in the last year of stellar evolution: setting the stage for the most luminous core-collapse supernovae

Raghunathan, S., et al. 2024, arXiv:2403.02337, Phys. Rev. Lett., 133, 121004, First Constraints on the Epoch of Reionization Using the Non-Gaussianity of the Kinematic Sunyaev-Zel'dovich Effect from the South Pole Telescope and Herschel-SPIRE Observations

Rani, B., et al. 2013, arXiv:1301.7087, Ast. and Ap., 552, A11, Radio to gamma-ray variability study of blazar S5 0716+714

Redman, R. O., Feldman, P. A., Matthews, H. E., Halliday, I., & Creutzberg, F. 1992, A. J., 104, 405, Millimeter and Submillimeter Observations of the Asteroid 4 Vesta

Refregier, A., Amara, A., Kitching, T. D., Rassat, A., Scaramella, R., & Weller, J. 2010, arXiv:1001.0061, arXiv e-prints, arXiv:1001.0061, Euclid Imaging Consortium Science Book

Remazeilles, M. & Chluba, J. 2024, arXiv:2410.02488, arXiv e-prints, arXiv:2410.02488, Evidence for relativistic Sunyaev-Zeldovich effect in Planck CMB maps with an average electron-gas temperature of $T_{\rm e} \simeq 5$ keV

Reuter, C., et al. 2020, arXiv:2006.14060, Ap. J., 902, 78, The Complete Redshift Distribution of Dusty Star-forming Galaxies from the SPT-SZ Survey

Richards, J. L., et al. 2011, arXiv:1011.3111, Ap. J. Supp., 194, 29, Blazars in the Fermi Era: The OVRO 40 m Telescope Monitoring Program

Ritacco, A., Boulanger, F., Guillet, V., Delouis, J.-M., Puget, J.-L., Aumont, J., & Vacher, L. 2023, arXiv:2206.07671, Ast. and Ap., 670, A163, Dust polarization spectral dependence from Planck HFI data. Turning point for cosmic microwave background polarization-foreground modeling

Schaan, E., et al. 2021, arXiv:2009.05557, Phys. Rev. D, 103, 063513, Atacama Cosmology Telescope: Combined kinematic and thermal Sunyaev-Zel'dovich measurements from BOSS CMASS and LOWZ halos

Schmittfull, M. & Seljak, U. 2018, arXiv:1710.09465, Phys. Rev. D, 97, 123540, Parameter constraints from cross-correlation of CMB lensing with galaxy clustering

Schöneberg, N., Abellán, G. F., Sánchez, A. P., Witte, S. J., Poulin, V., & Lesgourgues, J. 2022, arXiv:2107.10291, Phys. Rep., 984, 1, The H_0 Olympics: A fair ranking of proposed models

Shandera, S., et al. 2019, arXiv:1903.04700, BAAS, 51, 338, Probing the origin of our Universe through cosmic microwave background constraints on gravitational waves

Shariff, J. A., et al. 2019, arXiv:1809.06375, Ap. J., 872, 197, Submillimeter Polarization Spectrum of the Carina Nebula

Shiode, J. H. & Quataert, E. 2014, arXiv:1308.5978, Ap. J., 780, 96, Setting the Stage for Circumstellar Interaction in Core-Collapse Supernovae. II. Wave-driven Mass Loss in Supernova Progenitors

Shvartzvald, Y., et al. 2024, arXiv:2304.14482, Ap. J., 964, 74, ULTRASAT: A Wide-field Time-domain UV Space Telescope

Sierra, C. E., et al. 2025, arXiv:2405.06868, Ap. J. Supp., 276, 31, Simons Observatory: Predeployment Performance of a Large Aperture Telescope Optics Tube in the 90 and 150 GHz Spectral Bands

Sikivie, P. 1983, Phys. Rev. Lett., 51, 1415, Experimental Tests of the "Invisible" Axion

Simon, S. M., et al. 2018, Journal of Low Temperature Physics, 193, 1041, The Advanced ACTPol 27/39 GHz Array

Slosar, A., Mandelbaum, R., & Eisenstein, D. 2019a, arXiv:1903.12016, in BAAS, Vol. 51, 97

Slosar, A. et al. 2019b, arXiv:1903.09883, in BAAS, Vol. 51, 98

Smith, K. M., Madhavacheril, M. S., Münchmeyer, M., Ferraro, S., Giri, U., & Johnson, M. C. 2018, arXiv:1810.13423, arXiv e-prints, arXiv:1810.13423, KSZ tomography and the bispectrum

Smith, N. 2014, arXiv:1402.1237, ARRA, 52, 487, Mass Loss: Its Effect on the Evolution and Fate of High-Mass Stars

Smith, T. L., Poulin, V., & Amin, M. A. 2020, arXiv:1908.06995, Phys. Rev. D, 101, 063523, Oscillating scalar fields and the Hubble tension: A resolution with novel signatures

Soderberg, A. M., et al. 2006, astro-ph/0604389, Nature, 442, 1014, Relativistic ejecta from X-ray flash XRF 060218 and the rate of cosmic explosions

Spergel, D., et al. 2015, arXiv:1503.03757, arXiv e-prints, arXiv:1503.03757, Wide-Field InfrarRed Survey Telescope-Astrophysics Focused Telescope Assets WFIRST-AFTA 2015 Report

Spilker, J. S., et al. 2016, arXiv:1604.05723, Ap. J., 826, 112, ALMA Imaging and Gravitational Lens Models of South Pole Telescope—Selected Dusty, Star-Forming Galaxies at High Redshifts

SPT, DES Collaboration. 2024, arXiv:2311.07512, Open J. Astrophys., 7, astro.2311.07512, Galaxy Clusters Discovered via the Thermal Sunyaev-Zel'dovich Effect in the 500-square-degree SPTpol Survey

Su, T., et al. 2017, arXiv:1511.06770, MNRAS, 464, 968, On the redshift distribution and physical properties of ACT-selected DSFGs

Sunyaev, R. A. & Zeldovich, I. B. 1980, ARRA, 18, 537, Microwave background radiation as a probe of the contemporary structure and history of the universe

Sunyaev, R. A. & Zeldovich, Y. B. 1972, Comments on Astrophysics and Space Physics, 4, 173, The Observations of Relic Radiation as a Test of the Nature of X-Ray Radiation from the Clusters of Galaxies

Tandoi, C., et al. 2024, arXiv:2401.13525, Ap. J., 972, 6, Flaring Stars in a Nontargeted Millimeter-wave Survey with SPT-3G

Tanimura, H., Douspis, M., Aghanim, N., & Salvati, L. 2022, arXiv:2110.08880, MNRAS, 509, 300, Constraining cosmology with a new all-sky Compton parameter map from the Planck PR4 data

Tassis, K., et al. 2018, arXiv:1810.05652, arXiv e-prints, arXiv:1810.05652, PASIPHAE: A high-Galactic-latitude, high-accuracy optopolarimetric survey

The Pan-Experiment Galactic Science Group, et al. 2025, arXiv:2502.20452, arXiv e-prints, arXiv:2502.20452, Full-sky Models of Galactic Microwave Emission and Polarization at Sub-arcminute Scales for the Python Sky Model

Thorne, B., Dunkley, J., Alonso, D., & Næss, S. 2017, arXiv:1608.02841, MNRAS, 469, 2821, The Python Sky Model: software for simulating the Galactic microwave sky

Tingay, S. J., et al. 2013, arXiv:1206.6945, PASA, 30, e007, The Murchison Widefield Array: The Square Kilometre Array Precursor at Low Radio Frequencies

Turner, M. S. & Widrow, L. M. 1988, Phys. Rev. D, 37, 2743, Inflation-produced, large-scale magnetic fields

Urry, C. M. 1998, astro-ph/9702176, Advances in Space Research, 21, 89, Multiwavelength properties of blazars

Vacher, L., Aumont, J., Boulanger, F., Montier, L., Guillet, V., Ritacco, A., & Chluba, J. 2023, arXiv:2210.14768, Ast. and Ap., 672, A146, Frequency dependence of the thermal dust E/B ratio and EB correlation: Insights from the spin-moment expansion

van Marrewijk, J., et al. 2024, arXiv:2310.06120, Ast. and Ap., 689, A41, XLSSC 122 caught in the act of growing up: Spatially resolved SZ observations of a z = 1.98 galaxy cluster

Vargas, C., et al. 2023, arXiv:2310.17535, arXiv e-prints, arXiv:2310.17535, The Atacama Cosmology Telescope: Extragalactic Point Sources in the Southern Surveys at 150, 220 and 280 GHz observed between 2008-2010

Verde, L., Treu, T., & Riess, A. G. 2019, arXiv:1907.10625, Nature Astronomy, 3, 891, Tensions between the early and late Universe

Walker, S., et al. 2020, arXiv:1909.11569, Journal of Low Temperature Physics, 199, 891, Demonstration of 220/280 GHz Multichroic Feedhorn-Coupled TES Polarimeter

Webster, W. J., Johnston, K. J., Hobbs, R. W., Lamphear, E. S., Wade, C. M., Lowman, P. D., Kaplan, G. H., & Seidelmann, P. K. 1988, A. J., 95, 1263, The Microwave Spectrum of the Asteroid Ceres

Weiland, J. L., Addison, G. E., Bennett, C. L., Halpern, M., & Hinshaw, G. 2020, arXiv:1907.02486, Ap. J., 893, 119, An Examination of Galactic Polarization with Application to the Planck TB Correlation

Weiler, K. W., Panagia, N., Montes, M. J., & Sramek, R. A. 2002, ARRA, 40, 387, Radio Emission from Supernovae and Gamma-Ray Bursters

Whitehorn, N., et al. 2016, arXiv:1604.03507, Ap. J., 830, 143, Millimeter Transient Point Sources in the SPTpol 100 Square Degree Survey

Wittenmyer, R. A., et al. 2020, arXiv:1912.01821, MNRAS, 492, 377, Cool Jupiters greatly outnumber their toasty siblings: occurrence rates from the Anglo-Australian Planet Search

Ysard, N., et al. 2024, arXiv:2401.07739, Ast. and Ap., 684, A34, THEMIS 2.0: A self-consistent model for dust extinction, emission, and polarisation

Yuan, W., et al. 2015, arXiv:1506.07735, arXiv e-prints, arXiv:1506.07735, Einstein Probe - a small mission to monitor and explore the dynamic X-ray Universe

Yurk, N. Y., Ravi, V., & Ho, A. Y. Q. 2022, arXiv:2206.03518, Ap. J., 934, 5, Models of Millimeter and Radio Emission from Interacting Supernovae

Zauderer, B. A., et al. 2011, arXiv:1106.3568, Nature, 476, 425, Birth of a relativistic outflow in the unusual γ-ray transient Swift J164449.3+573451

Zeldovich, Y. B. & Sunyaev, R. A. 1969, APSS, 4, 301, The Interaction of Matter and Radiation in a Hot-Model Universe

Zhang, B. T., Murase, K., Kimura, S. S., Horiuchi, S., & Mészáros, P. 2018, arXiv:1712.09984, Phys. Rev. D, 97, 083010, Low-luminosity gamma-ray bursts as the sources of ultrahigh-energy cosmic ray nuclei

Zhu, N., et al. 2021, arXiv:2103.02747, Ap. J. Supp., 256, 23, The Simons Observatory Large Aperture Telescope Receiver

Zonca, A., Singer, L., Lenz, D., Reinecke, M., Rosset, C., Hivon, E., & Gorski, K. 2019, Journal of Open Source Software, 4, 1298, healpy: equal area pixelization and spherical harmonics transforms for data on the sphere in Python, https://doi.org/10.21105/joss.01298

Zonca, A., Thorne, B., Krachmalnicoff, N., & Borrill, J. 2021, Journal of Open Source Software, 6, 3783, The Python Sky Model 3 software, https://doi.org/10.21105/joss.03783

A Sensitivity and forecasting assumptions

Table 1 provides map-domain sensitivities for the full-depth maps expected at the conclusion of the SO LAT survey in 2034. To obtain these numbers, we take a similar approach to that in Ade et al. (2019), using an atmospheric noise model informed by ACT observations combined with detector NET sensitivities estimated using `bolocalc` (Hill et al. 2018). For the nominal-survey SO forecasts described in Ade et al. (2019), it was assumed that 20% of the data collected over a 5-year duration would be usable for cosmological analysis (after accounting for uptime, CMB field availability, and data quality cuts, all of which were estimated based on historical data from ACT). For this work, we use the same detector NET sensitivities and 20% observation efficiency, but make the following changes. Rather than assuming a 5-year survey with the OT configuration from Ade et al. (2019) (comprising 1 LF, 4 MF, and 2 UHF OTs), we assume 3 years of nominal SO observations with that tube configuration, followed by 6 years of observations with the fully populated LATR (comprising 1 LF, 8 MF, and 4 UHF OTs, as described in Sec. 2). Ade et al. (2019) assumed that the sky fraction observed would comprise $f_{\rm sky} = 0.47$, with a post-masking footprint of $f_{\rm sky} = 0.4$ available for cosmological analysis (avoiding regions of Galactic contamination and poor cross-linking near the footprint edges). In this work, following updates to the SO scan strategy that accommodate a wider range of science goals, we assume that throughout the 9-year survey duration the SO LAT will map a sky fraction $f_{\rm sky} = 0.61$. These assumptions lead to the full-depth map sensitivities given in Table 1. For completeness, we provide the "goal" and "baseline" per-OT NET sensitivities in Table 5. Further details for the cosmological science forecasts and the point-source and transient forecasts are given below.

Cosmology: All of our cosmological science forecasts use the "goal" sensitivity levels and assume that the sky fraction available for analysis after masking the Galaxy is $f_{\rm sky} = 0.4$. However, over this sky fraction, we have assumed slightly different map-domain sensitivities of $\{39, 20, 3.5, 3.8, 9.1, 22\}$ μK $\cdot$ arcmin at $\{27, 39, 93, 145, 225, 280\}$ GHz, respectively, compared to the values of $\{44, 23, 3.8, 4.1, 10, 25\}$ μK $\cdot$ arcmin given in Table 1, due to different survey-strategy assumptions that were made earlier in the cosmological analyses. These small differences in the map-domain noise levels are not expected to significantly change our cosmological forecasts at the precision level quoted in this work.

Transient and point source science: We use two types of sensitivities for our transient and point source forecasts. First, we estimate our sensitivities to point sources from a single observation, that is, for a point on the sky that drifts once through the entire focal plane, which is scanning in azimuth at a fixed elevation. We base these sensitivities on simulated

Table 5. SO Large Aperture Telescope NET per Optics Tube

Band	LF1	LF2	MF1	MF2	UHF1	UHF2
Frequency [GHz]	27	39	93	145	225	280
Baseline NET [$\mu K\sqrt{s}$]	48	24	10.8	13.4	21.2	50.9
Goal NET [$\mu K\sqrt{s}$]	35	18	7.8	8.4	14.1	35.4

Forecasts in this work and in Ade et al. (2019) are based on "baseline" and "goal" noise models. This table provides the associated NET per OT; note that each OT includes three ∼150-mm detector arrays. The baseline model represents the requirements for SO, while goal represents the expected performance. These models include parameters to encapsulate the key drivers for instrumental sensitivity, including: the emission from and opacity of the atmosphere; the properties of the telescope (emission, spill, etc.); properties of the receiver and cryogenic optics (emission, losses, and reflections from the windows, lenses, and cryogenic cold stop); properties of the filters that define the passbands; and detector properties (yield, noise, etc.). The sensitivities presented here were computed at the start of the design process, when many instrumental details were yet to be finalized. For this reason, the parameter choices are uninformative and are not reported here. Pre-deployment testing of the MF OTs indicates performance exceeding the baseline requirement and consistent with goal performance (Sierra et al. 2025).

maps made with our nominal observing strategy, in which the majority of observations occur at 40° elevation (70.6% of observations), with a minority at 50° (15.7%) and at 60° (13.7%). We use a fixed set of detector NETs for these simulations, and we then rescale the maps to correspond to the NETs used for the full-depth cosmological forecasts listed in Table 1. We take the median map depth, in units of $\mu K \cdot$ arcmin, for each of the observing elevations, and calculate their weighted mean based on the observing fraction at each elevation. Second, we estimate our sensitivities to point sources in the final, full-survey maps by spreading the array sensitivity accumulated over the survey duration over the survey area, using $f_{\rm sky} = 0.61$ and an observing efficiency of 20%, as described above. For both single-observation and full-depth maps, we obtain point source sensitivities by converting the map depth in $\mu K \cdot$ arcmin to mJy using the beam FWHMs listed in Table 1 and applying an inverse-variance weighting with an atmospheric $1/\ell$ noise spectrum with a power-law index of -3.5 and $\ell_{\rm knee} = \{500, 500, 2100, 3000, 3800, 3800\}$ for $\{27, 39, 93, 145, 225, 280\}$ GHz, respectively. Here, the $\ell_{\rm knee}$ values are estimated based on ACT data.[12] For the full-depth maps, we include additional "noise" contributions from the CMB and the CIB, since these terms dominate over the atmospheric noise in this case (other background sources like unresolved AGN are ignored). We ignore these terms for the single-observation maps since they are subdominant. The resulting sensitivities for both the single-observation and full-survey cases are given in Table 3.

[12]Note that Ade et al. (2019) also made use of a set of $\ell_{\rm knee}$ values for the noise model used in forecasts (which is used in the cosmological forecasting in this paper as well), but there the term would have been better called a *reference* multipole, $\ell_{\rm ref}$, rather than a *knee* multipole, which is usually defined as the multipole where the red noise caused by the atmosphere reaches the same level as the white noise; Ade et al. (2019) instead defined a "red noise" amplitude, $N_{\rm red}$, to scale the reference multipole. The relationship between the two is: $N_{\rm red}/\ell_{\rm ref}^{\alpha} = \sigma^2/\ell_{\rm knee}^{\alpha}$, where α is the power-law index of the red noise. For the point source forecasts in this paper, our choices of $\ell_{\rm knee}$ and α are independent of the model used in Ade et al. (2019), but are still chosen to be consistent with the atmospheric noise measured by ACT.